X-ray Absorption, Mössbauer, and EPR Studies of the Dinuclear Iron Center in the Hydroxylase Component of Methane Monooxygenase

Jane G. DeWitt,[†] James G. Bentsen,[‡] Amy C. Rosenzweig,[‡] Britt Hedman,[§] Jeffrey Green,[⊥] Simon Pilkington,[⊥] Georgia C. Papaefthymiou,[∥] Howard Dalton,*[,⊥] Keith O. Hodgson,*[,†] and Stephen J. Lippard*[,‡]

Contribution from the Department of Chemistry, Stanford University, Stanford, California 94305, Department of Chemistry, Massachusetts Institute of Technology, Cambridge, Massachusetts 02139, Stanford Synchrotron Radiation Laboratory, Stanford University, Stanford, California 94309, Department of Biological Sciences, University of Warwick, Coventry CV4 7AL, United Kingdom, and Francis Bitter National Magnet Laboratory, Massachusetts Institute of Technology, Cambridge, Massachusetts 02139.
Received March 14, 1991

Abstract: The dinuclear iron center of the hydroxylase component (protein A) of methane monooxygenase isolated from *M. capsulatus* (Bath) has been studied by EXAFS, Mössbauer, and EPR spectroscopy. Highly purified hydroxylase, which exhibits a featureless visible absorption spectrum above 300 nm, has been obtained. Analysis of the Fe K-edge EXAFS data for the hydroxylase in the oxidized Fe(III)Fe(III) state gives an Fe···Fe distance of 3.42 Å and an average first shell Fe–O/N distance of 2.04 Å. Three of four oxidized hydroxylase samples investigated were photoreduced by the X-ray beam to give an EPR detectable mixed-valent Fe(II)Fe(III) form of the enzyme with $g_{av} = 1.83$. For these mixed-valent samples, an Fe···Fe distance of 3.41–3.43 Å and an average first shell Fe–O/N distance of 2.06–2.09 Å were determined. The EXAFS data for the photoreduced *M. trichosporium* OB3b hydroxylase are similar to those obtained for the *M. capsulatus* (Bath) samples, suggesting that the two proteins contain similar diiron cores. The absence of a short Fe–O distance indicates that the hydroxylase does not contain an oxo bridge. In addition, the results of the first shell fits suggest that the iron atoms are coordinated to more oxygen than nitrogen donor ligands. From a study of the power saturation behavior of the EPR spectrum obtained for the photoreduced *M. capsulatus* (Bath) sample, an antiferromagnetic exchange coupling constant $J = -32$ cm^{-1} was measured. This value is consistent with the presence of a monodentate ligand such as hydroxo, alkoxo, or monodentate carboxylato bridging the Fe(II)Fe(III) center and with the presence of at least one other bridging group, most likely a *syn,syn* bidentate carboxylate. For Fe(II)Fe(II) hydroxylase EXAFS samples, 85% in the fully reduced state as judged by Mössbauer spectroscopy, no resolvable Fe···Fe interaction could be detected, and an average first shell Fe–O/N distance of 2.15 Å was obtained. The Fe K-edge EXAFS spectrum of the diferric model complex $[Fe_2O(O_2CH)_4(BIPhMe)_2]$ was also obtained and compared to the protein data. Contrary to our earlier work, we have found that the best fit Fe···Fe distance of the hydroxylase samples is dependent on the model compound used to determine parameters for data analysis. The potential consequences of this finding to the analysis of EXAFS data obtained for other iron oxo proteins is discussed.

Introduction

Methane serves as the sole source of carbon and energy for obligate methanotrophic bacteria,[1] which are found between anaerobic methanogenic sediments and the oxidizing atmosphere associated with the evolutionarily more advanced photosynthetic bacteria.[2] The conversion of methane to methanol, which is the most chemically difficult step in this pathway, is catalyzed by the enzyme methane monooxygenase (MMO),[3] eq 1. MMO re-

$$CH_4 + O_2 + NADH + H^+ \rightarrow CH_3OH + H_2O + NAD^+ \quad (1)$$

ductively activates dioxygen for incorporation into a wide variety of hydrocarbon substrates, including alkanes, alkenes, aromatic and alicyclic hydrocarbons, phenols, alcohols, amines, and chlorinated hydrocarbons.[4,5] The extraordinary lack of specificity for methane monooxygenase resembles that for liver mitochondrial cytochrome P-450[6] and has probably been developed and retained because of its survival value to the bacteria in environments containing a wide range of natural and xenobiotic pollutants.[7] Unlike cytochromes P-450, the hydroxylase activity of methane monooxygenase is associated with a novel non-heme dinuclear iron center,[3,8,9] which is currently under investigation in our laboratories and elsewhere.[10,11]

Methane monooxygenase exists in two distinct forms in methanotrophic bacteria, a soluble non-heme iron enzyme and a copper-containing membrane-bound enzyme also believed to contain iron.[12] While the factors controlling the cellular location

[†] Stanford University.
[‡] Department of Chemistry, Massachusetts Institute of Technology.
[§] Stanford Synchrotron Radiation Laboratory.
[⊥] University of Warwick.
[∥] Francis Bitter National Magnet Laboratory, Massachusetts Institute of Technology.

(1) Anthony, C. *The Biochemistry of the Methylotrophs*; Academic Press: London, 1982.
(2) Whittenbury, R.; Phillips, K. C.; Wilkinson, J. F. *J. Gen. Microbiol.* **1970**, *61*, 205–218.
(3) Dalton, H. *Adv. Appl. Microbiol.* **1980**, *26*, 71–87.
(4) (a) Colby, J.; Stirling, D. I.; Dalton, H. *Biochem. J.* **1977**, *165*, 395–402. (b) Hou, C. T.; Patel, R. N.; Laskin, A. I.; Barnabe, N. *FEMS Microbiol. Lett.* **1980**, *9*, 267–270. (c) Leak, D. J.; Dalton, H. *J. Gen. Microbiol.* **1983**, *129*, 3487–3497. (d) Burrows, K. J.; Cornish, A.; Scott, D.; Higgins, I. J. *J. Gen. Microbiol.* **1984**, *130*, 3327–3333.
(5) Fox, B. G.; Borneman, J. G.; Wackett, L. P.; Lipscomb, J. D. *Biochemistry* **1990**, *29*, 6419–6427.
(6) Ortez de Montellano, P. R., Ed. *Cytochrome P-450: Structure, Mechanism, and Biochemistry*; Plenum Press: New York, 1986.
(7) Higgins, I. J.; Best, D. J.; Hammond, R. C.; Scott, D. *Microbiol. Rev.* **1981**, *45*, 556–590.
(8) Woodland, M. P.; Dalton, H. *J. Biol. Chem.* **1984**, *259*, 53–59.
(9) Prince, R. C.; George, G. N.; Savas, J. C.; Cramer, S. P.; Patel, R. N. *Biochim. Biophys. Acta* **1988**, *952*, 220–229.
(10) (a) Woodland, M. P.; Patil, D. S.; Cammack, R.; Dalton, H. *Biochim. Biophys. Acta* **1986**, *873*, 237–242. (b) Ericson, A.; Hedman, B.; Hodgson, K. O.; Green, J.; Dalton, H.; Bentsen, J. G.; Beer, R. H.; Lippard, S. J. *J. Am. Chem. Soc.* **1988**, *110*, 2330–2332. (c) DeWitt, J.; Hedman, B.; Ericson, A.; Hodgson, K. O.; Bentsen, J.; Beer, R.; Lippard, S. J.; Green, J.; Dalton, H. *Physica B* **1989**, *158*, 97–98. (d) Liu, K. E.; Lippard, S. J. *J. Biol. Chem.* **1991**, *266*, 12836–12839.
(11) (a) Fox, B. G.; Surerus, K. K.; Münck, E.; Lipscomb, J. D. *J. Biol. Chem.* **1988**, *263*, 10553–10556. (b) Fox, B. G.; Lipscomb, J. D. *Biochem. Biophys. Res. Commun.* **1988**, *154*, 165–170. (c) Fox, B. G.; Froland, W. A.; Dege, J. E.; Lipscomb, J. D. *J. Biol. Chem.* **1989**, *264*, 10023–10033.
(12) (a) Dalton, H.; Prior, S. D.; Leak, D. J.; Stanley, S. H. *Microbial Growth on C-1 Compounds, Proc. Int. Symp., 1983*; Amer. Soc. Microbiol.: Washington, D.C., 1984; pp 75–82. (b) Prior, S. D.; Dalton, H. *J. Gen. Microbiol.* **1985**, *131*, 155–163. (c) Akent'eva, N. P.; Stukan, R. A.; Prusakov, V. E.; Tsuprun, V. L.; Gvozdev, R. I.; Shushenacheva, E. V. *Biocatalysis* **1990**, *4*, 39–53.

0002-7863/91/1513-9219$02.50/0

of MMO have not been fully resolved, copper limitation[4d,13] or nonlimiting oxygen tensions[14] favor expression of the soluble enzyme. Under oxygen-limiting conditions, some methanotrophs possess extensive intracytoplasmic membranes, which support particulate MMO activity and exhibit distinguishing morphologies for the type I and type II organisms.[15] Under methane- or nitrate-limiting conditions (i.e. not oxygen-limiting conditions), few of these membranes are seen and soluble MMO activity predominates. Alternatively, as a result of copper limitation in a low copper medium, one can achieve a distinct switch from particulate to soluble activity with increasing biomass.[12a] While little is known about the particulate enzyme,[12c,16] substantial purification of soluble methane monooxygenase has been reported for several type I and type II methanotrophs.[8,11b,c,17] While these two classes of methanotrophs utilize different pathways for carbon assimilation, it is becoming increasingly clear that the soluble MMOs from both sources exhibit comparable chemical and physical properties.

Soluble methane monooxygenase has been purified to homogeneity from the representative type I organism *Methylococcus capsulatus* (Bath) and from the representative type II organism *Methylosinus trichosporium* OB3b. In the former case, MMO activity requires reconstitution of the holoenzyme from three isolable subunits. Component A, hereafter designated the hydroxylase component, has a $\alpha_2\beta_2\gamma_2$ polypeptide arrangement with M_r = 250 kDa for *M. capsulatus* (Bath), based on the recently published gene sequence,[18] and contains 2 to 4 nonheme iron atoms depending on the conditions of growth, harvesting, and purification. Recent studies of a very high specific activity hydroxylase from *M. trichosporium* OB3b have determined that the hydroxylase is the site of monooxygenase activity and that oxygenase activity is associated with the fully reduced form of the protein.[11c] Component B (M_r = 16 kDa) serves a regulatory function and lacks prosthetic groups.[19] Component C (39 kDa for *M. capsulatus* (Bath) based on gene sequence) contains one FAD and one Fe_2S_2 cluster that rapidly accept electrons from NADH.[20] Stopped flow kinetic studies implicate component C as the reductase component responsible for electron transfer from NADH to the hydroxylase.[21] Methane monooxygenase isolated from the type II organism *Methylobacterium* CRL-26 is very similar, although component B was reportedly not present.[17c,d]

EPR studies[10a] of the hydroxylase component of *M. capsulatus* (Bath) have suggested that the protein belongs to the class of dinuclear iron oxo proteins which includes hemerythrin (Hr), an oxygen transport protein, ribonucleotide reductase (RR), which converts ribonucleoside diphosphate to deoxyribonucleoside diphosphate for DNA synthesis, and purple acid phosphatase (PAP), which hydrolyzes phosphate esters.[22] Hemerythrin and ribonucleotide reductase are particularly relevant to the MMO problem since each contains a crystallographically characterized dinuclear iron center that interacts directly with dioxygen. Hr and MMO function as non-heme analogues of hemoglobin and cytochrome P-450, respectively. Factors controlling the transport (Hr) or reductive activation (MMO) of dioxygen are poorly understood for these non-heme Fe systems.

In an attempt to establish a structural basis for the different reactivity properties of the iron centers in MMO and Hr, we initiated a collaborative program to characterize the former by extended X-ray absorption fine structure (EXAFS) spectroscopy. EXAFS spectroscopy has proved to be very sensitive to the presence or absence of oxo bridges in dinuclear iron proteins and model compounds.[23] Most notably, the EXAFS modulations of oxo-bridged diferric model complexes are remarkably similar to one another and distinctively different from those of hydroxo-bridged diiron(III) models. Also, the short iron–oxo distance of the $\{Fe_2O\}^{4+}$ core in model compounds and proteins is well-resolved from the longer first shell N/O ligands in fits to the EXAFS data, and a short Fe–O contribution (at ~1.8 Å) is required to obtain satisfactory agreement with experiment.[23]

Oxidized and reduced hydroxylase of MMO from *M. capsulatus* (Bath) and oxidized hydroxylase from *M. trichosporium* OB3b have been previously investigated by EXAFS spectroscopy.[10b,c] Oxidized protein samples from these experiments were photoreduced by the X-ray beam to give an EPR detectable mixed-valent Fe(II)Fe(III) form of the enzyme. Analysis of EXAFS data on this semimet form indicated that it does not contain an oxo bridge in its dinuclear iron center. An EXAFS study on oxidized hydroxylase of MMO from *Methylobacterium* CRL-26 did not conclusively determine the presence or absence of an oxo or hydroxo bridge, owing to the limited k range of the EXAFS data, although the Fe···Fe distance reported (3.05 Å) was in the range of those found for some oxo-bridged models and proteins.[9]

In the present paper, we describe improved purification methods for the hydroxylase from *M. capsulatus* (Bath) and present a detailed structural characterization of the iron center in three oxidation states by EXAFS, Mössbauer, and EPR spectroscopy. We report Fe K-edge EXAFS measurements and analysis on newly prepared samples of oxidized and reduced hydroxylase from *M. capsulatus* (Bath). We were able to obtain EXAFS data on the diferric form of the protein, observing no photoreduction during the course of the experiment. We present a more complete analysis of the data reported earlier on the reduced and semimet protein samples, including a sample of the hydroxylase from the type II organism *M. trichosporium* OB3b. In addition, we report Fe K-edge EXAFS measurements and analysis on the diferric model $[Fe_2O(O_2CH)_4(BIPhMe)_2]$.[24]

Experimental Section

Bacterial Growth. *Methylococcus capsulatus* (Bath) was maintained under methane and air (1:3 (v/v)) at 45 °C in both our Warwick and M.I.T. laboratories by using a low copper, potassium nitrate mineral salts (NMS) medium, pH 6.8,[13] supplemented with 2.5 mg/L of $Na_2MoO_4 \cdot 2H_2O$. Organisms were subcultured biweekly on NMS non-nutrient agar slopes.[2] Solution cultures (50 mL) were subcultured every 3 weeks in stoppered 250-mL conical flasks, which were charged with the methane/air mixture and stored in a shaking orbital incubator (Series 25, New Brunswick Scientific Co., Edison, NJ) at 100 rpm and 45 °C. Commercial and technical grade methane was used as the principal carbon source (Air Products and British Oxygen Co.).

Cells for samples **EXAFS1–EXAFS3** and **EXAFS5** (for sample summary, see Table I) were prepared from *M. capsulatus* (Bath) isolated from a 100-L batch culture at Warwick (growth I). Cells for **EXAFS6** and the EPR samples were prepared from a 10-L continuous culture at M.I.T. (growth II). Mössbauer samples **a** and **b** were isolated from an ^{57}Fe-enriched 10-L batch culture at M.I.T. (growth III). Cell densities were monitored by light scattering (optical density, OD, measured at 540

(13) Stanley, S. H.; Prior, S. D.; Leak, D. J.; Dalton, H. *Biotechnol. Lett.* **1983**, *5*, 487–492.
(14) (a) Scott, D.; Brannan, J.; Higgins, I. J. *J. Gen. Microbiol.* **1981**, *125*, 63–72. (b) Scott, D.; Best, D. J.; Higgins, I. J. *Biotechnol. Lett.* **1981**, *3*, 641–644.
(15) (a) Davies, S. L.; Whittenbury, R. *J. Gen. Microbiol.* **1970**, *61*, 227–232. (b) Colby, J.; Dalton, H.; Whittenbury, R. *Annu. Rev. Microbiol.* **1979**, *33*, 481–517.
(16) (a) Smith, D. D. S.; Dalton, H. *Eur. J. Biochem.* **1989**, *182*, 667–671. (b) Akent'eva, N. P.; Gvozdev, R. I. *Biokhimiya* **1988**, *53*, 91–96. (c) Korshunova, L. A.; Akent'eva, N. P.; Gvozdev, R. I.; Shushenacheva, E. V. *Biokhimiya* **1989**, *54*, 1652–1657.
(17) (a) Colby, J.; Dalton, H. *Biochem. J.* **1978**, *171*, 461–468. (b) Woodland, M. P.; Dalton, H. *Anal. Biochem.* **1984**, *139*, 459–462. (c) Patel, R. N.; Savas, J. C. *J. Bacteriol.* **1987**, *169*, 2313–2317. (d) Patel, R. N. *Arch. Biochem. Biophys.* **1987**, *252*, 229–236.
(18) Stainthorpe, A. C.; Murrell, J. C.; Salmond, G. P. C.; Dalton, H.; Lees, V. *Arch. Microbiol.* **1989**, *152*, 154–159.
(19) Green, J.; Dalton, H. *J. Biol. Chem.* **1985**, *260*, 15795–15801.
(20) (a) Colby, J.; Dalton, H. *Biochem. J.* **1978**, *171*, 461–468. (b) Colby, J.; Dalton, H. *Biochem. J.* **1979**, *177*, 903–908. (c) Lund, J.; Woodland, M. P.; Dalton, H. *Eur. J. Biochem.* **1985**, *147*, 297–305.
(21) Green, J.; Dalton, H. *Biochem. J.* **1989**, *259*, 167–172.
(22) (a) Lippard, S. J. *Angew. Chem., Int. Ed. Engl.* **1988**, *27*, 344–361. (b) Sanders-Loehr, J. *Iron Carriers and Iron Proteins*; VCH Publishers Inc.: New York, 1989; pp 373–466. (c) Que, L., Jr.; Scarrow, R. C. *Metal Clusters in Proteins*; ACS Symposium Series No. 372; American Chemical Society: Washington, D.C., 1988; pp 152–178. (d) Vincent, J. B.; Olivier-Lilley, G. L.; Averill, B. A. *Chem. Rev.* **1990**, *90*, 1447–1467.
(23) Hedman, B.; Co, M. S.; Armstrong, W. H.; Hodgson, K. O.; Lippard, S. J. *Inorg. Chem.* **1986**, *25*, 3708–3711.
(24) (a) Tolman, W. B.; Bino, A.; Lippard, S. J. *J. Am. Chem. Soc.* **1989**, *111*, 8522–8523. (b) Tolman, W. B.; Liu, S.; Bentsen, J. G.; Lippard, S. J. *J. Am. Chem. Soc.* **1991**, *113*, 152–164.

Table I. EXAFS Sample and Data Collection Summary

sample no.	description	data collection information[a]	scans averaged/ scans collected
EXAFS1[b]	*M. capsulatus* oxidized → semimet	Jan 1987; SSRL 2-2; Si(111); 10 K; focussed	22/32
EXAFS2[b]	*M. capsulatus* oxidized → semimet	Nov 1987; SSRL 4-2; Si(111); 10 K; focussed	22/32
EXAFS3	*M. capsulatus* reduced	Nov 1987; SSRL 4-2; Si(111); 10 K; focussed	24/29
EXAFS4[b]	*M. trichosporium* oxidized → semimet	Nov 1987; SSRL 4-2; Si(111); 10 K; focussed	6/13
EXAFS5	*M. capsulatus* oxidized	June 1989; NSLS X19A; Si(220); Sept 1989; NSLS X19A; Si(111); 10 K, unfocussed	199/235[c]
EXAFS6	*M. capsulatus* reduced	Sept 1989; NSLS X19A; Si(111); 10 K; unfocussed	228/260[c]

[a] SSRL, Stanford Synchrotron Radiation Laboratory. NSLS, National Synchrotron Light Source. For all samples run at SSRL, an ionization chamber of the Stern/Lytle design[32] was used to detect the fluorescence. [b] Sample was photoreduced to the semimet state by the X-ray beam. Only the scans after photoreduction was complete were averaged for further analysis. [c] The Ge solid-state array detector has 13 elements. Each time the sample is scanned, 13 individual data files are collected. The 235 files collected for **EXAFS5** represent 12 individual scans of the sample with 12 channels collected (June 1989) and 7 individual scans of the sample with 13 channels collected (September 1989); the 260 files collected for **EXAFS6** represent 20 individual scans of the sample with 13 channels collected.

nm). For growth I, 10 L of a continuous culture with OD = 8 were used to inoculate a 100-L fermenter (L.H. Engineering Ltd, Stokes Poges, Bucks, U.K.) as described previously.[4a] The cells were harvested in batch culture when the OD reached 12 by using a Westfalia continuous centrifuge (Westfalia Separator Ltd., Wolverton, Bucks, U.K.). At M.I.T., freshly batched subculture flasks were used to inoculate a 10-L Microfirm fermenter (New Brunswick Scientific Co.) which was then operated in either batch or continuous culture at 45 °C. As the growth proceeded, the stir rate and gas flow rates were increased over the ranges of 400–600 rpm, 40–50 mL/min of methane, and 150–200 mL/min of air at 15 psig. Continuous cultures were initiated late in log phase (OD = 8–12) at a dilution rate of 0.05 h^{-1}. In growths II and III, cells were harvested by using a Pennwalt tubular bowl centrifuge to yield an average of 8 g of cell paste per liter of culture media. Cells used in Mössbauer studies (growth III) were enriched with ^{57}Fe by replacing the usual Fe content of the growth media with 95% ^{57}Fe-enriched $Na_2[Fe(EDTA)]$, prepared from Fe foil (U.S. Services Inc., Summit, NJ). The 10-L batch culture was harvested when the OD reached 9, yielding 50 g of cell paste. After each culture was harvested, cells were washed with cold 20 mM sodium phosphate buffer at pH 7.0 (5 mL of buffer/g of cell paste) and centrifuged at 10000 × *g* for 20 min. The cell paste (growths II and III) or its cell free extract (growth I) was stored at −80 °C.

Preparation of Cell Free Extract. Cell paste was suspended in 20 mM Tris/HCl (growth I) or in 25 mM MOPS (MOPS = 3-[N-morpholino]propanesulfonic acid) (growth II and III) buffer at pH 7.0 (2 mL of buffer/g of cell paste) containing 5 mM sodium thioglycolate to stabilize the reductase,[17a] 0.01 mg/mL of DNAse I, 0.5 mM $MgCl_2$, and 1 mM phenylmethylsulfonyl fluoride as a serine protease inhibitor to protect protein B.[19] Cells were lysed with a French press at 137 MPa. The resulting lysate was centrifuged at 100000 × *g* for 90 min. The supernatant was carefully decanted and is hereafter referred to as the cell-free extract.

Purification of the Hydroxylase. *M. capsulatus* (Bath) hydroxylase protein for Mössbauer and X-ray absorption studies was purified at Warwick (**EXAFS1–EXAFS4**) and at M.I.T. (**EXAFS5** and **EXAFS6**, Mössbauer samples **a** and **b**, and EPR samples) by methods adapted from Woodland and Dalton.[8,17b] Typically, the cell-free extract was resolved into fractions A, B, and C by stepwise ion exchange chromatography (0.0, 0.2, and 0.5 M NaCl) on a DEAE cellulose column (4.5 × 7 cm) equilibrated in 20 mM Tris/HCl at pH 7.0 or 25 mM MOPS at pH 7.0 containing 5 mM sodium thioglycolate. The hydroxylase (ca. 100 mg/mL) did not bind to the DEAE cellulose and was further purified in 2-mL portions by high-performance liquid chromatography (HPLC) with an Ultrapak TSKG3000SWG (Pharmacia) gel filtration column (21.5 mm × 600 mm). At Warwick, the HPLC column was equilibrated with 25 mM (**EXAFS1**) or 50 mM (**EXAFS2** and **EXAFS3**) Tris/HCl buffer at pH 7.0. Pooled hydroxylase fractions were supplemented with 25 mM or 50 mM PIPES (piperazine-*N*,*N*'-bis[2-ethanesulfonic acid]) buffer at pH 7.0, respectively, prior to freezing in liquid nitrogen and storage at −80 °C. For subsequent purifications at M.I.T., the HPLC column was equilibrated with a high ionic strength buffer (0.1 M NaCl in 50 mM MOPS at pH 7.0) which gave superior resolution of the hydroxylase. **EXAFS5**, **EXAFS6**, and Mössbauer samples **a** and **b** were prepared from protein purified in this manner.

Influenced by recent reports,[11b,c] we modified the hydoxylase purification protocol as follows. Cell free extract was resolved by stepwise ion exchange chromatography on DEAE cellulose. The hydroxylase was then applied to a DEAE Sepharose CL6B column, equilibrated in 25 mM MOPS at pH 7.0, and eluted with a 0–0.6 M NaCl gradient. The hydroxylase eluted at 0.2 M NaCl. Final purification was then carried out by size exclusion chromatography on Sephacryl S-300 equilibrated in 25 mM MOPS at pH 7.0. Optical and EPR measurements have been made on protein purified in this manner.

***Methylosinus trichosporium* OB3b Samples.** A culture of *Methylosinus trichosporium* OB3b was maintained on nitrate mineral salts agar plates[25] at Warwick[26] as previously described.[2] *M. trichosporium* OB3b was grown at 30 °C in oxygen-limited continuous culture at a dilution rate of 0.05 h^{-1} on ammonium mineral salts medium with methane (20% v/v in air) as the carbon source. *M. trichosporium* OB3b hydroxylase for **EXAFS4** was purified at Warwick according to methods outlined above for **EXAFS1–EXAFS3**. Specific activities were determined by using components B and C from *M. capsulatus* (Bath). Efficient cross reactivity has been established previously for these two organisms.[27]

Enzyme Assays. Hydroxylase activity was measured in the presence of saturating amounts of components B and C by using propylene as a substrate.[4a] The formation of propylene oxide was monitored gas chromatographically by using a 2.1 m wide bore glass column packed with Porapak Q (Alltech Associates). A unit (U) of activity is defined as 1 μmol of product/min. Small amounts of ethanol were removed from NADH (Sigma) used in activity assays by ether extraction (5×) in 20 mM potassium phosphate buffer at pH 7.0. The resulting solution was vacuum dried until free of ether as determined by gas chromatography. Purified NADH was stored as 1-mL aliquots at −20 °C.

Sample Preparations. Purified hydroxylase was typically concentrated by ultrafiltration on an Amicon PM 10 membrane, dialyzed into an appropriate glycerol or ethylene glycol containing buffer, and further concentrated on a Centricon (Amicon) centrifugal microconcentrator. Samples **EXAFS2–EXAFS4** and **EXAFS6** were degassed and transferred to an anaerobic wet box (vide infra). **EXAFS2** and **EXAFS4** samples were directly loaded into capped ca. 140 μL lucite EXAFS cells (23 mm × 2 mm × 3 mm) with 25 μm Kapton windows. **EXAFS3** and **EXAFS6** samples were chemically reduced to the diferrous form as described below. All samples were removed from the wet box, immediately submerged in liquid nitrogen, and subsequently stored in a liquid nitrogen refrigerator. EXAFS samples prepared from degassed 50% ethylene glycol buffers yielded high quality optical glasses when frozen. The use of glasses reduces the problem of Bragg diffraction peaks (arising from crystalline ice in the frozen samples) which can introduce glitches and other background abnormalities in the EXAFS data.

Mössbauer samples **a** and **b** were prepared from cells grown on ^{57}Fe-enriched media. HPLC purified protein was concentrated and dialyzed into appropriate buffers. Sample **a** was desalted by dialysis into 5% ethylene glycol buffer and then dialyzed into 50% ethylene glycol buffer to mimic the EXAFS sample medium. This sample was used to optimize conditions for chemical generation of the diferrous form of the hydroxylase for EXAFS spectroscopy experiments (see Anaerobic Reductive Titrations). Sample **b** was dialyzed into 20% ethylene glycol buffer and concentrated.

Protein Analytical Procedures. Protein purity and size were determined by denaturing polyacrylamide gel electrophoresis.[8] Protein concentrations were estimated by using the Bio-Rad assay, with bovine serum albumin as the standard. Iron was determined by flameless atomic absorption spectroscopy at 371.99 nm by using a Varian AA-1475 atomic

(25) Colby, J.; Dalton, H.; Whittenbury, R. *Annu. Rev. Microbiol.* **1979**, *33*, 481–517.
(26) Stirling, D. I.; Dalton, H. *Eur. J. Biochem.* **1979**, *96*, 205–212.
(27) Stirling, D. I.; Colby, J.; Dalton, H. *Biochem. J.* **1979**, *177*, 361–364.

absorption spectrometer and associated GTA-95 graphite tube atomizer. Results were in good agreement with those obtained spectrophotometrically by complexation of iron with ferrozine [3-(2-pyridyl)-5,6-bis(4-phenylsulfonic acid)-1,2,4-triazine].[28]

Anaerobic Reductive Titrations. Concentrated protein samples for physical studies were deoxygenated at 4 °C by slow successive evacuation (10^{-3} Torr, 5 min) and back flushing with 1 atm of Ar (5 min) on a vacuum line for six cycles. No loss of activity occurred as a result of this treatment. Deoxygenated samples under Ar were subsequently transferred to a Vacuum Atmospheres anaerobic chamber operated as a wet box. Oxygen levels were monitored with a Vacuum Atmospheres Model AO-316-C oxygen analyzer and maintained below 4 ppm during all sample manipulations. The mixed-valent hydroxylase sample for EPR spectroscopic study (166 μM, 1.7 Fe/protein) was prepared by addition of sodium dithionite (71 μM) in the presence of 100 μM phenazine methosulfate. The sample was incubated for 5 min at 25 °C and frozen in liquid nitrogen. In order to achieve full reduction, anaerobically prepared samples were incubated for 25 min with a 10-fold molar excess of sodium dithionite in the presence of 100 μM methyl viologen and 10 μM proflavin.

Mössbauer Spectroscopy. Zero-field Mössbauer spectra were recorded at 4.2 and 80 K by using a conventional constant acceleration spectrometer equipped with a temperature controller maintaining temperatures within ±0.1 K. The source was ^{57}Co in Rh. Isomer shifts are referred to Fe metal at room temperature. Data were collected for 96 h at 80K–100K counts per channel for protein samples containing approximately 40 μg of ^{57}Fe. Data were fitted with a sum of Lorentzian quadrupole doublets by using a least-squares routine.

EPR Spectroscopy. EPR spectra were recorded at X-band on a Bruker Model ESP 300 spectrometer with an Oxford Instruments EPR 900 liquid helium cryostat and a Bruker ER035M gaussmeter. The $g < 2$ signal for the $S = {}^1/_2$ mixed-valent form of the hydroxylase was quantitated under nonsaturating conditions by double integration of the first derivative spectrum with a frozen 1 mM solution of copper perchlorate (1 mM $CuSO_4$, 2 M $NaClO_4$, 0.01 M HCl) as standard. Spin quantitation of the $g = 4.3$ resonance was performed by using Na_2[Fe(EDTA)] as a standard. Transition probabilities were corrected for g-value anisotropy.[29] Frozen EXAFS samples were directly interrogated in EXAFS cells by using a home-built flow-through liquid-helium cryostat with an internal i.d. of 6 mm.

Power saturation studies were performed on the mixed-valent species in the photoreduced **EXAFS2** sample. For these experiments, the EXAFS sample was annealed and a 100-μL aliquot was transferred to a matched 3-mm EPR tube. A second EPR tube was fitted with a 100 Ω carbon resistor in 50% ethylene glycol for accurate temperature calibration of the cryostat according to standard methods. EPR absorption derivative signal intensities, I, at $g = 1.85$ were measured as a function of incident microwave power, $P = 100$ nW to 100 mW, at a variety of temperatures (5–12 K). $P_{1/2}$ was determined graphically at each temperature according to eq 2.[30]

$$\log (I/\sqrt{P}) = a - (b/2) \log (P_{1/2} + P) \quad (2)$$

Preparation of the Model Complex. The complex $[Fe_2O(O_2CH)_4(BIPhMe)_2]$ was synthesized as previously reported.[24] Samples for XAS measurements were diluted with BN and the mixture was ground to a fine powder. The model/BN mixture was pressed into a pellet (1.0 mm thick) supported by an Al spacer and held in place with 63.5 μm Mylar tape windows.

EXAFS Data Collection and Reduction. All protein sample data were measured in fluorescence mode at 10 K maintained by using an Oxford Instruments continuous-flow liquid-helium CF1208 cryostat. The **EXAFS1** sample (Table I) was run at SSRL on focussed beamline 2-2 during dedicated conditions (3 GeV, 50–65 mA) by using a Si(111) double-crystal monochromator tuned 100% at 7850 eV.[31] The fluorescence signal was detected with an Ar-filled ionization chamber,[32] equipped with Soller slits and a Mn filter. **EXAFS2**, **EXAFS3**, and **EXAFS4** samples (Table I) were run at SSRL on focussed wiggler beamline 4-2 during dedicated conditions by using a Si(111) double-crystal monochromator tuned 100% at 7968 eV, and the same detector setup as for **EXAFS1**. **EXAFS5** sample (Table I) was run at NSLS on unfocused beamline X19A (2.5 GeV, 90–200 mA) by using a Si(220) double-crystal monochromator detuned for harmonic rejection to 66% of the maximum at 7375 eV. The fluorescence signal was monitored by using a 13-element Ge solid-state array detector[33] windowed on the Fe Kα signal. During the experiment, count rates of approximately 37 000 s^{-1} (total per element) were measured at 7375 eV. The **EXAFS5** sample was again measured at NSLS on beamline X19A along with **EXAFS6** under the same conditions as the first **EXAFS5** experiment, except that a Si(111) double-crystal monochromator detuned to 50% of the maximum at 7820 eV was employed. Count rates of approximately 28 000 s^{-1} (total per element) at 7800 eV were measured for the Ge detector during this experiment. The model compound was measured in transmission mode at 10 K with use of N_2-filled ionization chambers of standard design. The sample was run at SSRL (3 GeV, 50–80 mA) on unfocussed wiggler beamline 7-3 by using a Si(220) double-crystal monochromator detuned 50% at 7997 eV.

Data reduction was performed according to methods described in detail elsewhere[34] but briefly summarized here. Energies were calibrated by using an internal iron foil standard,[35] assigning the first inflection point of the Fe absorption edge as 7111.2 eV. Calibrated scans were inspected individually and rejected if the signal-to-noise level was too high compared to the other scans as a result of beam instabilities or poor detector statistics, or because a beam loss occurred during the scan. In the case of the photoreduced samples **EXAFS1**, **EXAFS2**, and **EXAFS4**, the edge shifted during the first approximately 4 h of irradiation. These scans were excluded from the subsequent weighted average of scans used in the data analysis.

The same oxidized protein sample (**EXAFS5**) was run twice with different monochromators (Table I), giving rise to different background functions and glitch effects. Photoreduction of this oxidized protein sample did not occur, either because of the lower incident flux at NSLS compared to SSRL or because the new purification procedure used for this particular sample removed impurities that mediated the photoreduction for samples **EXAFS1**, **EXAFS2**, and **EXAFS4**. An average of **EXAFS5** data set was done separately (108/144 "scans" for the June 1989 data and 91/91 "scans" for the September 1989 data), the two averages were normalized to each other, and the EXAFS spectra of the two files were averaged before fits were performed on the merged data. Monochromator glitches were edited out of the **EXAFS5** individual averages, as well as the **EXAFS3** and **EXAFS6** average files, using a single-point replacement method (2, 4, and 2 points total edited, respectively). For the model compound $[Fe_2O(O_2CH)_4(BIPhMe)_2]$, 5 of 7 scans were averaged, and one glitch was edited out of the average.

A pre-edge subtraction was performed by fitting the EXAFS region with a smooth polynomial which was extrapolated into the pre-edge region and subtracted. A three-segment spline was fit to the EXAFS region and subtracted and the data normalized to an edge jump of one. The spline was chosen so that it minimized residual low-frequency background but did not reduce the EXAFS amplitude as checked by monitoring the Fourier transform of the EXAFS during the background subtraction process. The normalized, background-subtracted data were converted to k space, where k is the photoelectron wavevector defined by $[2m_e(E - E_0)/\hbar^2]^{1/2}$. In this expression, m_e is the electron mass, E the photon energy, $\hbar$ is Planck's constant divided by 2π, and E_0 is the threshold energy, 7130 eV (where k is defined to be 0).

EXAFS Data Analysis. Analysis was performed with nonlinear least-squares curve-fitting[34,35] techniques with empirical phase and amplitude parameters, as described previously.[34] The following models were used to obtain the empirical Fe–X backscattering parameters of interest: Fe–O and Fe–C from [Fe(acetylacetonate)$_3$];[36] Fe–N from [Fe(1,10-phenanthroline)$_3$]$(ClO_4)_3$;[37] Fe–Fe from $[Fe_2(OH)(OAc)_2(HBpz_3)_2](ClO_4)$[38a] (**FeOHFe-HBpz**) and $[Fe_2O(OAc)_2(HBpz_3)_2]$[38b] (**FeOFe-**

(28) (a) Massey, V. *J. Biol. Chem.* **1957**, *229*, 763. (b) Stookey, L. L. *Anal. Chem.* **1970**, *42*, 779–781.
(29) Aasa, R.; Vänngård, T. *J. Magn. Reson.* **1975**, *19*, 308–315.
(30) Yim, M. B.; Kuo, L. C.; Makinen, M. W. *J. Magn. Reson.* **1982**, *46*, 247–256.
(31) This is the same data set as reported in ref 10b; the data have been reanalyzed over the same range and with the same experimental phase and amplitude functions used for the samples reported in this paper for direct comparisons.
(32) (a) Stern, E. A.; Heald, S. M. *Rev. Sci. Instrum.* **1979**, *50*, 1579–1582. (b) Lytle, F. W.; Greegor, R. B.; Sandstrom, D. R.; Marques, E. C.; Wong, J.; Spiro, C. L.; Huffman, G. P.; Huggins, F. E. *Nucl. Instrum. Methods* **1984**, *226*, 542–548.
(33) Cramer, S. P.; Tench, O.; Yocum, M.; George, G. N. *Nucl. Instrum. Methods Phys. Res.* **1988**, *A266*, 586–591.
(34) (a) Cramer, S. P.; Hodgson, K. O.; Stiefel, E. I.; Newton, W. E. *J. Am. Chem. Soc.* **1978**, *100*, 2748–2761. (b) Cramer, S. P.; Hodgson, K. O. *Prog. Inorg. Chem.* **1979**, *15*, 1–39. (c) Scott, R. A. *Methods Enzymol.* **1985**, *117*, 414–459.
(35) Scott, R. A.; Hahn, J. E.; Doniach, S.; Freeman, H. C.; Hodgson, K. O. *J. Am. Chem. Soc.* **1982**, *104*, 5364–5369.
(36) (a) Iball, J.; Morgan, C. H. *Acta Crystallogr.* **1976**, *23*, 239–244. (b) Roof, R. B., Jr. *Acta Crystallogr.* **1956**, *9*, 781–786.
(37) Johansson, L. *Chem. Scr.* **1976**, *9*, 30–35. The crystal structure of the perchlorate salt has not been determined, but the $[Fe(phenanthroline)_3]^{2+}$ complex structure can be assumed to be identical with that of the corresponding iodide salt (Johansson, L.; Molund, M.; Oskarsson, A. *Inorg. Chim. Acta* **1978**, *31*, 117–123).

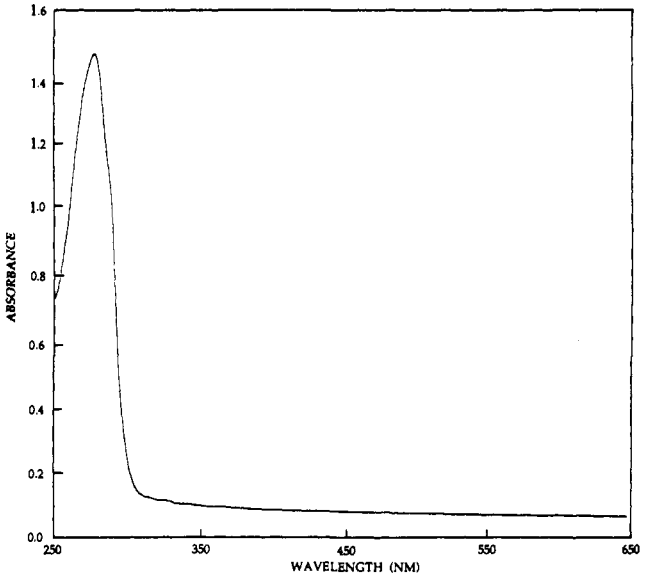

Figure 1. Optical spectrum of the *M. capsulatus* (Bath) hydroxylase (1 mg/mL).

HBpz). Data for these model compounds were collected as described previously.[10b]

For all the data presented, Fourier transforms (from k to R space) of 3.5–12.5 and 3.5–10.8 Å^{-1} were performed and two data ranges, from 4.0–12.0 and 3.8–10.0 Å^{-1}, respectively, were fit. A Gaussian window of 0.1 Å was used for all transforms. The window widths used in the backtransforms (from R to k space) are listed in the figures and tables. They were kept as similar as possible to each other, as well as to the windows used to extract amplitude and phase parameters from the models, to minimize artifacts introduced by the Fourier filtering technique. All curve fitting was based on k^3-weighted data and applied to individual filtered shells as well as to wide-range filtered shells and to the raw data. Only the structure-dependent parameters, i.e. the distance and the number of atoms in the shell, were varied except where otherwise noted. For example, in the first shell fits the same Debye–Waller factor as determined for the models was used in fitting the proteins and the coordination number was varied. A "goodness-of-fit" parameter, F, was calculated as $F = \{[k^6(\text{data} - \text{fit})^2]/(\text{no. of points})\}^{1/2}$ for each fit.

Results

Protein Purification. Soluble hydroxylase was isolated by eluting cell-free extract with stepwise increases in salt concentration from a DEAE cellulose ion exchange chromatography column. The hydroxylase was further purified by using a HPLC gel filtration column. For protein purified in Warwick (samples **EXAFS1–EXAFS4**), chromatographic resolution on the latter column was poor and never approached that reported previously.[17b] Denaturing polyacrylamide gel electrophoresis (PAGE) showed contaminating methanol dehydrogenase (MDH), and specific activities were typically around 130 mU/mg. Satisfactory resolution by HPLC required a high ionic strength buffer, in contrast to the original report.[17b] Ionic strength effects of this type have been reported previously.[39] Hydroxylase obtained in this manner was pure by PAGE and exhibited specific activities typically in the 100–300 mU/mg range, but we have observed a value as high as 550 mU/mg with 2 Fe per protein.

By utilizing methods recently described,[11c] we have, as mentioned, further improved resolution and efficiency of the hydroxylase isolation procedure. The crude hydroxylase fraction from the DEAE cellulose column was applied to a DEAE-Sepharose CL6B column and eluted with a salt gradient. MDH eluted with no addition of salt, while the hydroxylase was displaced at 0.2 M NaCl, effectively separating the two proteins. The crude extract can also be loaded directly onto the Sepharose column and the hydroxylase, protein B, and the reductase eluted with a 0–0.6 M NaCl gradient. The hydroxylase, essentially pure at this stage, was freed of residual cytochrome by gel filtration on Sephacryl S-300 to give hydroxylase which was pure by all standards. Protein samples purified by this procedure contained 2–4 Fe/protein and exhibited specific activities of 100–300 mU/mg.

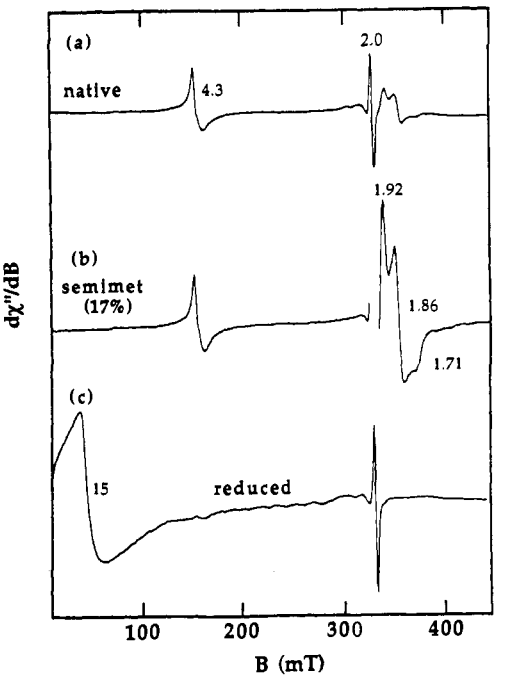

Figure 2. X-band EPR spectra of the *M. capsulatus* (Bath) hydroxylase (42 mg/mL, 166 μM, 1.7 Fe/protein): (a) oxidized, 1 mW, (b) mixed valent (see Anaerobic Reductive Titrations), 1 mW, (c) fully reduced, 50 mW. Instrumental conditions were the following: scan range, 600 mT; field set, 305 mT; time constant, 83 ms; modulation amplitude, 8.0 mT; modulation frequency, 100 kHz; scan time, 3 min; 9 K; 9.44 GHz.

Optical Properties. Figure 1 shows the optical absorption spectrum of the purified hydroxylase from *M. capsulatus* (Bath). Aside from the protein absorption at 280 nm, there were no significant optical features that could definitely be attributed to the iron prosthetic group. This result disagrees with previous reports of a feature at 410 nm attributable to purified protein from *M. capsulatus* (Bath)[8] and *Methylobacterium* CRL-26, respectively.[17c] Protein purified by us, employing the original literature procedure,[8,17b] exhibited such a feature along with weak accompanying spectral features at 521 and 550 nm. Chemical reduction of these samples increased all three absorbances and effected a bathochromic shift of the high-energy feature to 415 nm, suggesting the presence of cytochrome impurity. We have minimized the presence of such impurities in our newly purified protein and observe no other features beyond 300 nm, which is consistent with the recent results for the hydroxylase isolated from *M. trichosporium* OB3b.[11c]

EPR Spectroscopy and Chemical Reductions of the Hydroxylase. Figure 2 shows EPR spectral data for the hydroxylase from *M. capsulatus* (Bath). As described previously for both type I[9,10a] and type II[9,11a] organisms, native hydroxylase is essentially EPR silent. The weak $g = 4.3$ signal is associated with mononuclear ferric ion and accounts for less than 5% of the Fe present in the sample. Intensities of the $g = 2$ signal are variable and do not correlate with activity.[10a,11a] The weak rhombic signal at $g_{av} = 1.83$ (1.92, 1.86, 1.71) is characteristic of a Zeeman split $S = {}^1/_2$ ground state of an antiferromagnetically coupled mixed valent Fe(II)Fe(III) center. Integration of the $g_{av} = 1.83$ signal reveals the presence of the mixed valent state in less than 2% abundance, based on dinuclear iron centers. Chemical reduction of native hydroxylase with dithionite in the presence of phenazine methosulfate mediator results in an increase in the $g_{av} = 1.83$ signal, but we were unable to achieve high conversion to the mixed valent state with the conditions described in the Experimental Section. In Figure 2b we present the EPR spectrum obtained after 5 min

(38) (a) Armstrong, W. H.; Lippard, S. J. *J. Am. Chem. Soc.* **1984**, *106*, 4632–4633. (b) Armstrong, W. H.; Spool, A.; Papaefthymiou, G. C.; Frankel, R. B.; Lippard, S. J. *J. Am. Chem. Soc.* **1984**, *106*, 3653–3667.

(39) Kelner, D. N.; Mayhew, J. W.; Hobbs, J. B. *ABL* **1989**, February, 40.

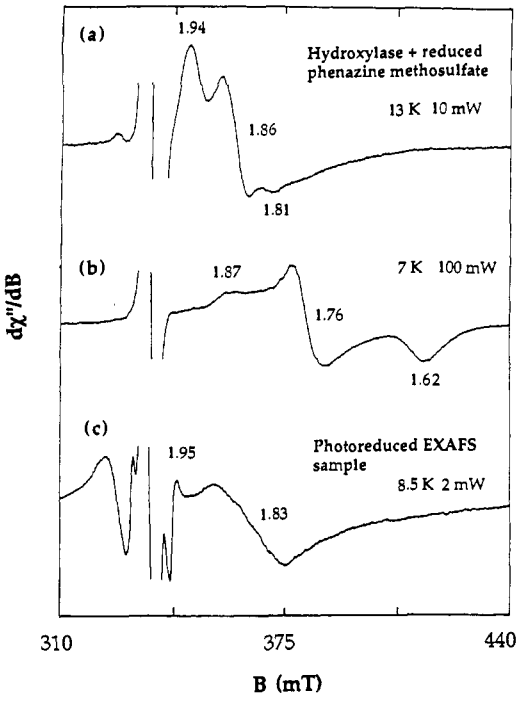

Figure 3. X-band EPR spectra for the *M. trichosporium* OB3b hydroxylase: (a) chemically reduced using dithionite and the mediator phenazine methosulfate, (b) same, (c) photoreduced **EXAFS4**. Instrumental conditions were the following: scan range, 400 mT; field set, 377 mT; time constant, 167 ms; modulation amplitude, 4.0 mT; modulation frequency, 100 kHz; scan time, 6 min; 9.43 GHz.

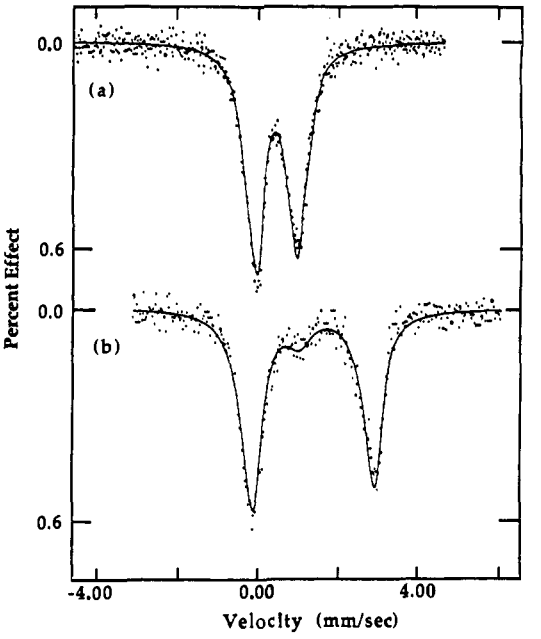

Figure 4. Mössbauer spectrum of the *M. capsulatus* (Bath) hydroxylase at 80 K and zero applied field (282 mg/mL, 0.6 mM, 1.3 Fe/protein): (a) oxidized, (b) fully reduced (see Sample Preparations and Anaerobic Reductive Titrations). Cells grown on ^{57}Fe enriched media.

of incubation of the *M. capsulatus* hydroxylase, showing only 17% conversion of dinuclear iron centers to the mixed valent state. The $g = 4.3$ signal intensity does not change. Importantly, mixed valent hydroxylase generated by dithionite reduction of native hydroxylase exhibits a single rhombic $g < 2$ EPR signal with line shape that is independent of applied microwave power and temperature. Furthermore, the signal is the same as that obtained upon X-ray photoreduction of hydoxylase in the EXAFS beam (vide infra). Midpoint potentials for the appearance and disappearance of the EPR signature for the Fe(II)Fe(III) state during redox titration of the hydroxylase were originally reported at 350 and −25 mV vs NHE.[11a] Phenazine methosulfate, which has a redox potential of 85 mV,[40] should therefore buffer the solution potential and optimize generation of the mixed valent state. A recent redetermination of the midpoint potentials, however, yielded values of 48 and −135 mV, respectively, for the Fe(III)Fe(III)/Fe(II)Fe(III) and Fe(II)Fe(III)/Fe(II)Fe(II) redox couples.[10d] These results indicate that phenazine methosulfate is not an optimal mediator for producing the mixed valent hydroxylase, affording a theoretical maximum yield of only 22% upon stoichiometric addition of dithionite.

Use of phenazine methosulfate as a mediator was previously shown to result in the generation of two distinct mixed valent states of the hydroxylase from *Methylococcus* CRL-25 and *Methylobacterium* CRL-26,[9] distinguishable by different power saturation behavior characteristics. In contrast, a single mixed valent state was observed for the *M. capsulatus* hydroxylase reduced in the presence of phenazine methosulfate. We have also reinvestigated the chemical reduction of the hydroxylase from *M. trichosporium* OB3b and find that, with phenazine methosulfate, signals arise from two mixed valent species, one seen at temperatures near 15 K and 10 mW of applied microwave power (Figure 3a) (g_{av} = 1.87, g = 1.94, 1.86, 1.81) and the second best observed at lower temperature and larger applied powers (Figure 3b) (g_{av} = 1.75; g = 1.87, 1.76, 1.62). At low temperature, the g_{av} = 1.87 signal saturates readily and follows a Curie law temperature dependence, but the g_{av} = 1.75 signal could not be saturated even at the highest powers. A g_{av} = 1.75 signal strongly resembling the g_{av} = 1.75 signal we observed has been reported recently for the *M. trichosporium* OB3b hydroxylase in the presence of protein B.[41] It thus seems likely that our samples of the *M. trichosporium* OB3b hydroxylase, purified at Warwick, may have contained small amounts of protein B. Correspondingly, sample **EXAFS4** may have contained some protein B. Furthermore, the two mixed valent species for the hydroxylase from *Methylococcus* CRL-25 and *Methylobacterium* CRL-26[9] probably represent hydroxylase free and complexed with protein B. If this interpretation is correct, MMO from these two organisms would contain component B, in contrast to previous reports.[17c,d]

The fully reduced form of the hydroxylase exhibits a signal at g = 15 (Figure 2c) similar to that reported for *M. trichosporium* OB3b.[11a,c,42] The extent of reduction was judged both by this EPR signal (4.2 K) and by the Mössbauer spectrum (δ = 1.06 mm/s, ΔE_Q = 3.01 mm/s, T = 80 K) of samples reduced in the presence of methyl viologen and proflavin. Addition of a 10-fold molar excess of dithionite in the presence of these two mediators reproducibly generated the diferrous form of the enzyme in greater than 85% yield. This chemical reduction procedure was used to prepare the reduced protein samples (**EXAFS3** and **EXAFS6**) for EXAFS analysis. After the EXAFS experiments, these samples were found to retain the g = 15 EPR signal.

Mössbauer Spectroscopy. The Mössbauer spectra of the oxidized and fully reduced forms of the hydroxylase from *M. capsulatus* (Bath) are shown in Figure 4. The spectrum of the oxidized protein recorded at zero field was fit with one quadrupole doublet having ΔE_Q = 1.05 mm/s and an isomer shift δ of 0.50 mm/s. The spectrum could also be fit with two doublets, for which $\Delta E_Q(1)$ = 0.95 mm/s, $\Delta E_Q(2)$ = 1.47 mm/s, $\delta(1)$ = 0.48 mm/s, $\delta(2)$ = 0.55 mm/s, without significant improvement of the fit. Similar observations have been recently reported for the *M. trichosporium* OB3b hydroxylase.[11a] No Fe^{2+} was evident in the sample, indicating that the hydroxylase, as isolated, is in the oxidized state. The 80 K Mössbauer spectrum of the reduced hydroxylase was fit with two quadrupole doublets, one associated with 15% unreacted oxidized protein and a second with parameters

(40) Prince, R. C.; Linkletter, S. J. G.; Dutton, P. L. *Biochim. Biophys. Acta* **1981**, *635*, 132–148.

(41) Fox, B. G.; Liu, Y.; Dege, J. E.; Lipscomb, J. D. *J. Biol. Chem.* **1991**, *266*, 540–550.

(42) Hendrich, M. P.; Münck, E.; Fox, B. G.; Lipscomb, J. D. *J. Am. Chem. Soc.* **1990**, *112*, 5861–5865.

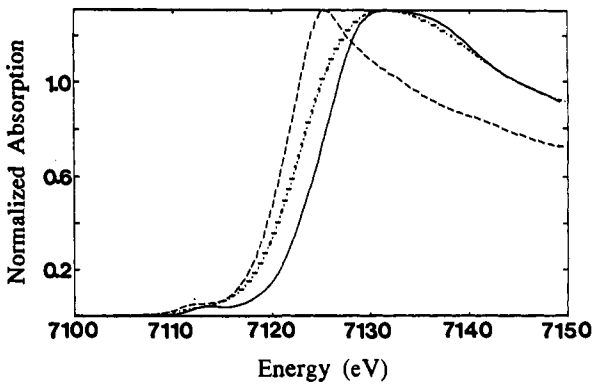

Figure 5. The Fe K X-ray absorption edge position of diferric (—), photoreduced semimet (- - -), and diferrous (- - -) hydroxylase of MMO from *M. capsulatus* (Bath).

typical of high-spin Fe^{2+}. This second doublet, which represents 85% of the total Fe in the sample, has ΔE_Q = 3.01 mm/s and an isomer shift δ = 1.30 mm/s. No second heterogeneous component appeared in the Mössbauer of the fully reduced form, as was reported for the reduced hydroxylase from *M. trichosporium* OB3b.[11a] The higher quadrupole splitting reported for the *M. trichosporium* OB3b hydroxylase[11a] (3.14 mm/s at 4.2 K) is probably a temperature effect associated with the weakly coupled system. Such a temperature dependence has been reported for diferrous model compounds.[43]

Photoreduction of the Oxidized Hydroxylase. The edge position of three oxidized hydroxylase samples (**EXAFS1**, **EXAFS2**, and **EXAFS4**) shifted approximately 1.5 eV to lower energy during the first four hours of exposure to the X-ray beam. This energy shift is due to 1 e^- photoreduction of the samples to the mixed valent state. For the same sample runs, the simultaneous Fe foil calibrations ensured that these shifts were well outside any experimental error. In Figure 5 are presented edge data for the nonphotoreduced, oxidized protein sample (**EXAFS5**), a dithionite reduced diferrous protein sample (**EXAFS6**), and a photoreduced protein sample (**EXAFS2**). The difference in sharpness of the edges arises from beamline-dependent resolution differences (Table I) and does not affect the observation that the edge shifts to lower energy by about 1.5 eV per added electron.

EPR measurements were made of EXAFS sample cells before and after X-ray exposure. The observed Fe K-edge shifts (−1.4 to −1.7 eV) correlated with photoreduction of the sample as monitored by the efficient accumulation of signals arising from a free radical (g = 2.0) and an $S = {}^1/_2$ mixed-valent dinuclear iron center ($g < 2.0$). For the **EXAFS2** sample, warmup to 298 K followed by recooling the EXAFS cell in the helium cryostat resulted in loss of the g = 2.0 signal without significant decline in the intensity of the Fe(II)Fe(III) signal (g = 1.92, 1.86, 1.71). Subsequent spin integration revealed ~60 ± 10% conversion to the mixed-valent state. This sample was subsequently transferred to an EPR tube for power saturation studies which supported the presence of a single mixed valent species. EPR studies also indicated extensive X-ray photoreduction of the **EXAFS4** sample containing *M. trichosporium* OB3b hydroxylase. Attempts to anneal this sample resulted in considerable precipitation of the protein. Estimates of the extent of photoconversion of the *M. trichosporium* OB3b hydroxylase to the mixed valent state (>70%) were made by estimating the contribution of the $g < 2$ signal to the integrated spectral density prior to annealing.

The EPR spectra for the photoreduced and chemically generated mixed-valent forms of the hydroxylases from both organisms were also compared. For the *M. capsulatus* (Bath) hydroxylase, a single mixed-valent species was observed for material generated by both photoreduction and dithionite reduction. In contrast, the *M. trichosporium* OB3b photoreduced sample **EXAFS4** exhibited the EPR spectrum shown in Figure 3c, which is different from

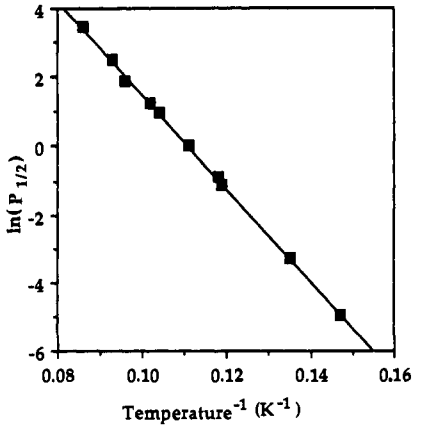

Figure 6. Dependence of the EPR half-saturation power, $P_{1/2}$, on absolute temperature for the photoreduced *M. capsulatus* (Bath) sample **EXAFS2**.

that reported for chemically reduced hydroxylase from this organism. This g = 1.83 signal was found to be independent of applied microwave power over a temperature range of 4.2–17 K, and is thought to be associated with a single species. When the photoreduced sample **EXAFS4** was warmed to room temperature and recooled, the protein precipitation was accompanied by conversion to no fewer than three mixed-valent species, one probably due to the interaction of the hydroxylase with a small amount of protein B.

Microwave Power Saturation Studies of the Mixed-Valent Hydroxylase. The power saturation behavior of the photoreduced *M. capsulatus* (Bath) sample **EXAFS2** was investigated at temperatures ranging from 5 to 12 K. The broadening parameter $b/2$ and the half saturation power $P_{1/2}$ were determined graphically as the asymptotic slope and intercept, respectively, in accord with eq 2. For relaxation dominated by phonon-assisted coupling of the ground and first excited states (the Orbach process),[30] the temperature dependence of the EPR half-saturation power can be related to the energy separation between the ground and first excited state, Δ, by eq 3, where k is the Boltzmann constant and A is a constant for the system. To validate the assumption implicit

$$\ln P_{1/2} = \ln A - \Delta/kT \qquad (3)$$

in the derivation of eq 3 that spin–spin (T_2) contributions to microwave susceptibility are negligible, we make the following observations. While the homogeneous spin-packet line width is determined by T_2, we see no change in line shape with microwave power saturation or temperature. Second, the broadening parameter ($b/2$), reflecting the ratio of Lorentzian spin-packet width and Gaussian envelope width, is independent of temperature. To rule out the case where $T_1 > T_2 \gg 1/\gamma H_1$, we established that $P_{1/2}$ was independent of modulation amplitude. A plot of ln $P_{1/2}$ as a function of temperature is shown in Figure 6, from which Δ = 96 cm^{-1} was determined for photoreduced *M. capsulatus* (Bath) hydroxylase. For isotropic exchange interaction between the two high-spin iron ions in an Fe(II)Fe(III) center, $\hat{\mathcal{H}}_{ex} = -2J\hat{S}_{5/2}\cdot\hat{S}_2$ and for $-J < 0$, the eigenstates of $\hat{\mathcal{H}}_{ex}$ are a ground doublet, a quartet at an energy $\Delta = -3J$, a sextet at $-5J$, etc. We realize that for some systems the exchange interaction is not much larger than the zero-field splitting expected for the two spins and inclusion of this term ($\hat{\mathcal{H}} = \hat{\mathcal{H}}_{ex} + \hat{\mathcal{H}}_{zfs}$) gives rise to a splitting of the quartet into two doublets with energies Δ_1 and Δ_2.[44] Nevertheless, we attach significance to the experimental value of Δ for comparative purposes as an indicator of the nature of intervening ligands. The energy and symmetry of these ligand orbitals are crucial determinants of the antiferromagnetic contribution to exchange, as evaluated by the magnitude of J. The derived coupling constant, $J \approx -32$ cm^{-1}, which has been reported previously,[24b] indicates weak antiferromagnetic exchange, con-

(43) Borovik, A. S.; Hendrich, M. P.; Holman, T. R.; Münck, E.; Papaefthymiou, V.; Que, L., Jr. *J. Am. Chem. Soc.* **1990**, *112*, 6031–6038.

(44) Sage, J. T.; Debrunner, P. G. *Hyperfine Interact.* **1986**, *29*, 1399–1402.

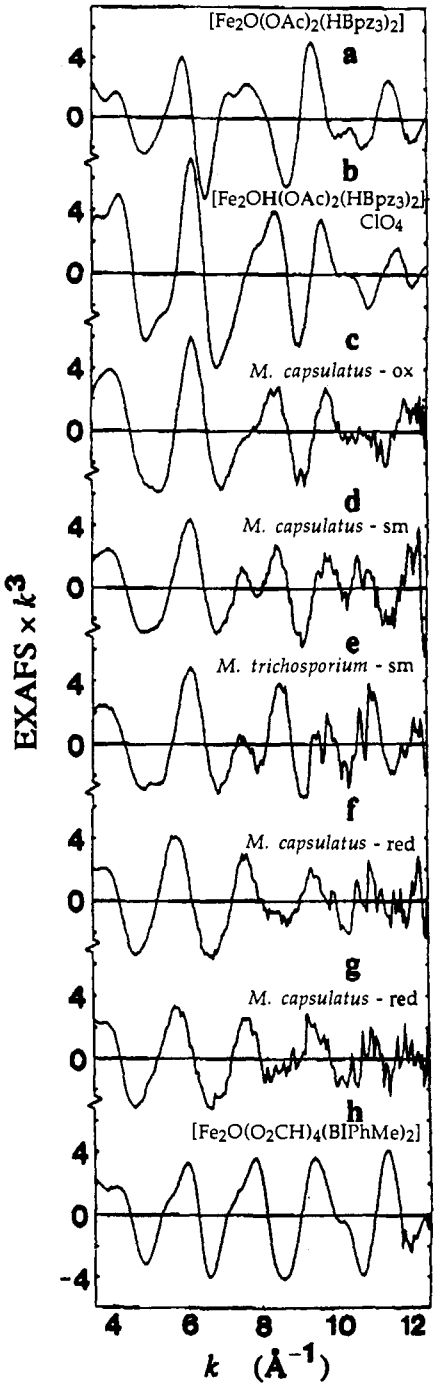

Figure 7. EXAFS data of the hydoxylase of MMO and binuclear iron model compounds: (a) **FeOFe–HBpz**, (b) **FeOHFe–HBpz**, (c) **EXAFS5**, (d) **EXAFS2**, (e) **EXAFS4**, (f) **EXAFS3**, (g) **EXAFS6**, (h) [$Fe_2O(O_2CH)_4$(**BIPhMe**)$_2$]. The data shown are the data used for Fourier transforms (k = 3.5–12.5 Å^{-1}) and fits.

sistent with hydroxo, alkoxo, or possibly monodentate carboxylato[24] bridging in the dinuclear iron core. This value agrees with the coupling constant $J \approx -30$ cm^{-1} recently reported for the *M. trichosporium* OB3b hydroxylase.[41] Values for J have been determined similarly for Fe(II)Fe(III) centers in deoxyHrNO (−23 cm^{-1}),[45] semimetHrN$_3$ (−15 cm^{-1}),[46] (semimet)$_R$Hr (−15 cm^{-1}),[46] and (μ-S^{2-})semimetHr (−29 cm^{-1}).[46]

X-ray Absorption Spectroscopy. The k^3-weighted EXAFS data of the protein samples **EXAFS2–EXAFS6** are presented in Figure

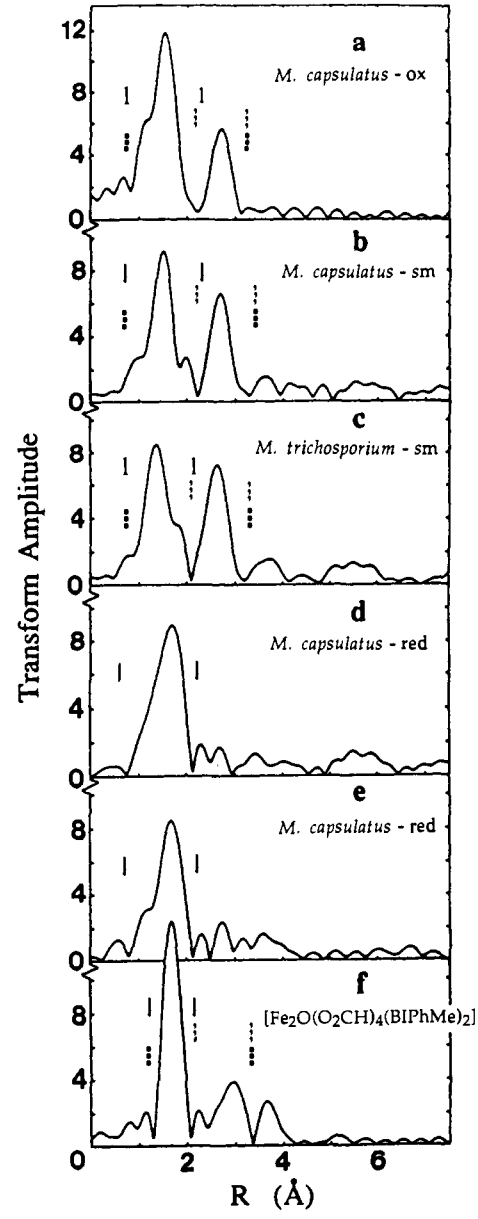

Figure 8. Fourier transforms of the EXAFS data presented in Figure 7 (c–h): (a) **EXAFS5**, (b) **EXAFS2**, (c) **EXAFS4**, (d) **EXAFS3**, (e) **EXAFS6**, (f) [$Fe_2O(O_2CH)_4$(**BIPhMe**)$_2$]. The bars on the figure represent the data backtransformed to R space for first (solid), second (dash), and wide shell fits (dot).

7c–g and the Fourier transforms in Figure 8a–e (for **EXAFS1**, see ref 10b). The oxidized protein EXAFS (Figure 7c) and the EXAFS of **FeOHFe–HBpz** (Figure 7b) show strong similarity, suggesting that the active site structure of the protein resembles that of the hydroxo-bridged model compound. The EXAFS of the semimet protein samples (Figure 7d,e) have maxima (at ~7 and 11 Å^{-1}) that are only shoulders in the oxidized protein sample EXAFS. The overall features of the EXAFS spectra of the semimet protein samples from the two bacterial species are similar, despite the higher noise level for the *M. trichosporium* OB3b sample (**EXAFS4**), as are the Fourier transforms indicating that the active sites of the hydroxylase from the two species are also comparable. The reduced protein EXAFS maximum around k = 6 Å^{-1} (Figure 7f,g) is shifted to lower k relative to the semimet and oxidized protein EXAFS, and the first shell peak in the Fourier transform is shifted to higher R (Figure 8d,e), suggesting that the first shell coordination around Fe is at a longer distance in the reduced form of the hydroxylase relative to the semimet and oxidized forms. Only one peak is seen in the Fourier transform of the reduced protein EXAFS; the peak attributed to Fe–Fe backscattering is absent, and the overall structure of the reduced

(45) Nocek, J. M.; Kurtz, D. M., Jr.; Sage, J. T.; Xia, Y.-M.; Debrunner, P.; Shiemke, A. K.; Sanders-Loehr, J.; Loehr, T. M. *Biochemistry* **1988**, *27*, 1014–1024.

(46) Pearce, L. L.; Kurtz, D. M., Jr.; Xia, Y.-M.; Debrunner, P. G. *J. Am. Chem. Soc.* **1987**, *109*, 7286–7293.

Table II. Results of First Shell Fits[a] to the Hydroxylase and Models

sample[b]	window width, Å	fit	N		O		
			CN[c]	*R*, Å	CN	*R*, Å	*F*[d]
EXAFS5	0.75–2.25	5A	3.4	2.02			1.0
M. capsulatus, ox		5B			3.0	1.99	0.73
		5C	2.3	2.14	3.5	1.97	0.35
		5D	2.7	1.95	3.0	2.06	0.41
EXAFS1	0.70–1.95	1A	3.0	2.03			0.70
M. capsulatus, sm		1B			2.5	2.00	0.61
		1C	1.6	2.22	3.2	2.00	0.37
		1D	3.7	2.01	1.5	2.14	0.37
EXAFS2	0.70–2.30	2A	2.3	2.03			0.97
M. capsulatus, sm		2B			2.0	2.01	0.83
		2C	2.5	2.20	3.1	1.99	0.25
		2D	3.4	1.99	2.4	2.13	0.23
EXAFS4	0.70–2.15	4A	1.7	2.02			1.2
M. trichosporium, sm		4B			1.6	2.00	1.1
		4C	3.0	2.16	2.8	1.96	0.55
		4D	3.0	1.96	2.8	2.09	0.48
EXAFS3	0.60–2.20	3A	3.2	2.14			0.87
M. capsulatus, red		3B			2.7	2.12	0.63
		3C	2.6	2.24	3.0	2.07	0.30
		3D	2.2	2.05	3.2	2.16	0.29
EXAFS6	0.70–2.20	6A	2.9	2.15			0.71
M. capsulatus, red		6B			2.5	2.12	0.50
		6C	1.9	2.25	2.7	2.09	0.26
		6D	1.9	2.07	2.6	2.17	0.27
FeOHFe–HBpz	0.85–2.10	A	4.6	2.04			1.0
		B			3.9	2.02	0.64
		C	2.9	2.13	3.8	1.98	0.27
		D	2.2	1.95	4.2	2.05	0.27
FeOFe–HBpz	1.20–2.15	E	3.7	2.12			0.62
		F			3.0	2.10	0.66
		G	3.5	2.12	0.5	1.74	0.45
		H			2.9	2.09	0.31
					0.7	1.76	
		I	1.4	2.24	3.4	2.07	0.15
					1.0	1.78	
		J	3.3	2.07	2.3	2.16	0.12
					0.95	1.79	

[a] Fitting range k = 4–12 Å^{-1}. Errors are estimated to be about ±0.03 Å for distances and 25% for coordination numbers.[34] [b] ox = oxidized; sm = semimet; red = reduced. [c] CN = coordination number. [d] F is defined in the Experimental Section.

protein EXAFS is less complicated than that of the semimet and oxidized protein EXAFS.

(a) First Shell Fits. Fourier-filtered EXAFS data were used in initial curve-fitting analysis, with window widths as indicated in Table II. A single O or N wave could not adequately fit the first shell EXAFS spectra for any of the hydroxylase samples, indicating that the first shell contains backscattering atoms at more than one distance and possibly of more than one type. Subsequent fits showed two different waves (O and N) to be necessary.[47] EXAFS spectroscopy cannot normally discriminate between backscatterers of similar strength as is the case with N and O (which differ only by one in atomic number); accordingly, two possible minima were found, one corresponding to $R_N > R_O$ and one to $R_N < R_O$, where R_N and R_O refer to the initial Fe–N and Fe–O bond lengths, respectively. Due to the limited k range of the data, the nitrogen and oxygen parameters were highly correlated and we therefore place a greater emphasis on the sum of coordination numbers and the coordination-weighted Fe–ligand distances than on individual values.

The validity of this approach was tested by performing the same fits on the two model compounds **FeOHFe–HBpz** and **FeOFe–HBpz**. The first shell data also could not be adequately fit by a single O or N wave. Fitting with both O and N waves gave the following coordination number sums and coordination-weighted Fe–ligand distances (for $R_N > R_O$): 6.7 N/O at 2.04 Å and 4.8 N/O at 2.12 Å, respectively, Table II. These values agree very well with the crystallographic averages, 6 N/O at 2.04 Å and 5 N/O at 2.12 Å.[38] With $R_N < R_O$ the corresponding results were 6.4 N/O at 2.02 Å and 5.6 N/O at 2.11 Å. As Fe–N bonds are generally longer than Fe–O bonds in dinuclear iron model compounds, the fit results with $R_N > R_O$ were used as the starting point in subsequent wide window fits.

Fits were also performed on all the protein samples to probe for the presence of a short (~1.80 Å) Fe–O distance, indicative of an oxo bridged center. When a short Fe–O distance was included, either negative coordination numbers resulted or the total oxygen contribution was split between two oxygen waves at distances on the order of 2.0 Å. Given the previously shown high sensitivity of EXAFS spectroscopy to the presence or absence of the short oxo bridge,[23] this result, together with the similarity of the oxidized and semimet hydroxylase EXAFS spectra to that of **FeOHFe–HBpz** and the dissimilarity to that of **FeOFe–HBpz** (Figure 7a–e), clearly indicates that the hydroxylase of methane monooxygenase does not have an oxo bridge in its dinuclear iron center.

For the oxidized hydroxylase sample (**EXAFS5**), an average first shell coordination of 5.8 N/O at 2.04 Å was found (Table II, fit 5C). Upon photoreduction to the semimet state, the first shell coordination distance increased to 4.8 N/O at 2.07 Å for **EXAFS1** (Table II, fit 1C), to 5.6 N/O at 2.08 Å for **EXAFS2** (Table II, fit 2C), and to 5.8 N/O at 2.06 Å for **EXAFS4** (Table II, fit 4C). The quality of the fits to the *M. trichosporium* OB3b

(47) This effect is due to interference in the EXAFS of O and N at different but unresolvable Fe–X distances. Fits by us and others (see ref 51) to structurally known model compounds have shown that using a single wave introduces systematic errors in the average bond length and unreasonable coordination numbers.

Table III. Results of Second Shell Fits[a] to the Hydroxylase

sample[b]	window width, Å	fit	Fe		C		
			CN[c]	R, Å	CN	R, Å	F[d]
EXAFS5	2.15–3.20	5E	1.1	3.42			0.40
M. capsulatus, ox		5F	0.7	3.04			0.65
		5G			5.3	3.05	0.31
		5H			3.8	3.39	0.78
		5I	1.4	3.45	3.9	3.32	0.33
		5J	0.5	3.38	4.0	3.07	0.22
		5K	0.3	2.96	5.4	3.06	0.23
EXAFS1	2.30–3.40	1E	1.0	3.43			0.46
M. capsulatus, sm		1F	0.6	3.05			0.65
		1G			4.8	3.07	0.41
		1H			3.9	3.40	0.71
		1I	1.2	3.47	4.6	3.34	0.36
		1J	0.6	3.38	4.1	3.10	0.30
		1K	0.3	2.97	5.0	3.08	0.35
EXAFS2	2.20–3.40	2E	1.1	3.41			0.61
M. capsulatus, sm		2F	0.8	3.04			0.73
		2G			6.0	3.05	0.38
		2H			4.7	3.39	0.85
		2I	1.6	3.47	7.4	3.33	0.44
		2J	0.5	3.35	5.7	3.07	0.31
		2K	0.02	2.98	5.8	3.06	0.35
EXAFS4	2.10–3.30	4E	1.3	3.41			0.72
M. trichosporium, sm		4F	1.1	3.04			0.71
		4G			7.3	3.04	0.34
		4H			4.8	3.38	1.09
		4I	2.4	3.46	10.1	3.31	0.41
		4J	0.09	3.37	7.0	3.04	0.34
		4K	0.4	3.02	6.0	3.04	0.25

[a] Fitting range k = 4–12 Å^{-1}. Errors are estimated to be about ±0.03 Å for distances and 25% for coordination numbers.[34] [b] ox = oxidized; sm = semimet. [c] CN = coordination number. [d] F is defined in the Experimental Section.

data is worse because of the higher noise level in the data compared to that of *M. capsulatus* (Bath) (only 6 scans were averaged for the *M. trichosporium* OB3b). The average first shell coordination of the reduced protein samples (**EXAFS3** and **EXAFS6**) was found to be 5.1 N/O at 2.15 Å (Table II, fits 3C and 6C). Although the average distance determined is the same for both reduced protein samples, the average coordination number for **EXAFS3** was more than 5 N/O while that for **EXAFS6** was less than 5 N/O, with the difference accounted for primarily in the coordination number of nitrogen.

(b) Second Shell Fits. The **FeOHFe–HBpz** compound was chosen as a model compound for extracting parameters to determine the Fe···Fe interaction in MMO for two reasons: first, in this compound the distribution of atoms in the second coordination sphere is such that the Fe···Fe distance is more isolated from second shell Fe···low-Z scatterer distances than in the analogous oxo-bridged model **FeOFe–HBpz** (the nearest C/N shell is about 0.25 Å away with only 2 O close to Fe in **FeOHFe–HBpz** whereas there are 8 C/N within 0.02–0.15 Å in **FeOFe–HBpz**[23]); second, since the first shell fits indicate that there is no oxo bridge in the iron protein center, a non-oxo-bridged model should provide more suitable parameters to use in fits of the protein active site.[48]

With the use of these empirical parameters in fits to the second shell data (Fourier transform windows are given in Table III) for hydoxylase samples **EXAFS1**, **EXAFS2**, **EXAFS4**, and **EXAFS5**, two Fe···Fe minima were found, one at ~3.0 Å and one at ~3.4 Å, depending on the initial Fe···Fe distance used in the fit. In a subsequent series of Fe-only fits, stepping the initial Fe···Fe distance value in intervals of 0.1 or 0.2 Å from 2.6 to 4.2 Å, it was found that the calculated iron wave moved into phase with the maximum of the amplitude envelope of the second shell data roughly every 0.4 Å, with the best fit (minimum in F and best similarity in shape) and maximum coordination number occurring at the 3.4 Å Fe···Fe distance for **EXAFS1**, **EXAFS2**, and **EXAFS5**. The same series of fits was performed by fixing the coordination number at 1 and varying the distance and the Debye–Waller factor, and a minimum in both F and the Debye–Waller factor was found at 3.4 Å (Figure 9) for **EXAFS1**, **EXAFS2**, and **EXAFS5**. For the noisier **EXAFS4** data the results were ambiguous, with the fits giving nearly equal preference to the 3.4 and 3.0 Å distances (see comment on shorter data range fits below). As shown in Table III, the two minima obtained for Fe-only fits for **EXAFS1**, **EXAFS2**, **EXAFS4**, and **EXAFS5** were essentially identical, 3.41–3.42 and 3.03–3.04 Å (Table III, fits 1E-F, 2E-F, 4E-F, and 5E-F).

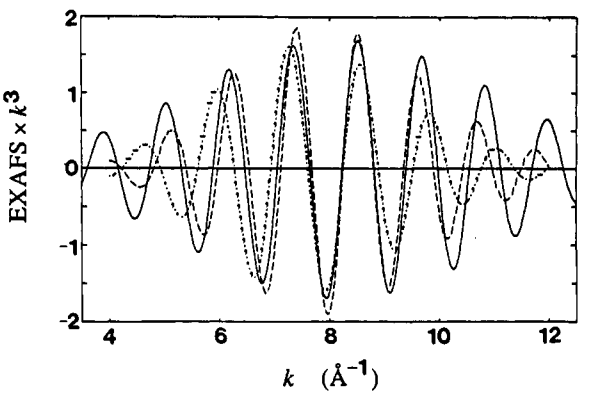

Figure 9. Fits to second shell data of **EXAFS5** with iron. The fits were done by fixing the coordination number at 1 and varying the distance and Debye–Waller factor. Second shell data (—), 3.42 Å fit (---), 3.03 Å fit (···).

It is difficult to obtain unique fits to second coordination sphere EXAFS spectra in dinuclear metalloproteins because the second shell generally contains carbon, nitrogen, and/or oxygen scatterers at radial distances near that of the metal–metal separation. If well-ordered, the contribution of 4–6 such low-Z scatterers can be approximately of the same magnitude as that of a single metal scatterer. Although the backscattering envelope from Fe should maximize at higher k values than envelopes from low-Z scatterers, interference among several shells of low-Z scatterers can effectively change the expected decreasing contribution to the EXAFS at higher k, and make the backscattering envelope of low-Z scatterers

(48) Zhang, K.; Stern, E. A.; Ellis, F.; Sanders-Loehr, J.; Shiemke, A. K. *Biochemistry* **1988**, *27*, 7470–7479.

Table IV. Results of Wide Shell Fits[a] to the Hydroxylase

sample[b]	window width, Å	fit	N		O		Fe		F[d]
			CN[c]	R, Å	CN	R, Å	CN	R, Å	
EXAFS5	0.75–3.20	5L	2.3	2.14	3.4	1.97			0.99
M. capsulatus, ox		5M	2.3	2.14	3.4	1.97	1.1	3.42	0.52
		5N	2.4	2.13	3.4	1.97	0.7	3.03	0.71
EXAFS1	0.70–3.40	1L	2.6	2.23	3.7	2.00			0.99
M. capsulatus, sm		1M	2.6	2.23	3.7	2.00	1.0	3.43	0.62
		1N	2.3	2.22	3.6	2.00	0.7	3.04	0.72
EXAFS2	0.70–3.40	2L	2.6	2.19	3.0	1.99			1.10
M. capsulatus, sm		2M	2.6	2.19	3.0	1.99	1.1	3.41	0.67
		2N	2.5	2.18	2.9	1.98	0.9	3.04	0.74
EXAFS4	0.70–3.30	4L	3.0	2.15	2.6	1.95			1.40
M. trichosporium, sm		4M	3.0	2.15	2.6	1.95	1.3	3.41	0.94
		4N	3.0	2.14	2.6	1.95	1.1	3.03	0.87

[a] Fitting range k = 4–12 Å^{-1}. Errors are estimated to be about ±0.03 Å for distances and 25% for coordination numbers.[34] [b] ox = oxidized; sm = semimet. [c] CN = coordination number. [d] F is defined in the Experimental Section.

appear quite similar to that of the metal.[49] The use of C backscattering parameters derived from Fe(acac)$_3$ to model the low-Z contribution to second shell data has often been described in the literature; however, its backscattering envelope is similar to that of a first row transition metal, most likely because of interference of its two closely lying C second shells. Moreover, low-Z contributions are difficult to model adequately because of the typical wide distribution of distances. It is, however, quite unlikely in any Fe coordination environment that outer C shells would be so ordered that they give an EXAFS contribution as large as those seen for the oxidized and semimet hydroxylase samples. For example, even in Fe(TPP), which has 8 well-ordered α-carbon atoms, the second shell peak in the Fourier transform is only about one-third the height of the first shell peak.[50]

For bridged dinuclear model compounds, the second coordination sphere normally contains a large number of low-Z atoms spread around 3.0 Å, always at a shorter distance than, and independent of, the Fe···Fe distance.[23] It would thus be expected that the strength of the 3.0 Å Fe···Fe distance minimum derives from accidental coincidence of the frequency decrease in the phase of the Fe wave with a distance where there is an actual strong contribution to the data from C/N/O backscatterers. The 3.4 Å distance, on the other hand, originates primarily from the Fe backscatterer, most likely mixed with other low-Z backscatterers. As has been pointed out elsewhere,[51] longer Fe···C distances are expected to contribute less distinctly to the EXAFS because they originate from three-bond Fe···C distances, and thus are expected to have high thermal disorder. Recognizing the difficulties in adequately fitting outer shells of C atoms, we nevertheless attempted C-only and Fe + C fits to the second shell data to compare with the Fe-only fits. C-only fits, as expected, revealed two principal Fe–C fit minima at ~3.0 and 3.4 Å (Table III, fits 1G-H, 2G-H, 4G-H, and 5G-H), with a strong preference for the minimum corresponding to the 3.0 Å distance. This 3.0 Å Fe–C minimum had a lower F value and was a somewhat better fit to the data than the 3.4 Å Fe-only fits for all samples. As described above, a factor making interpretation of these results more difficult is the fact that the C backscattering envelope is quite similar to that of Fe. This phenomenon has been observed by others; for example, see Table II in ref 51.[52]

Not surprisingly, when refined together, the iron and carbon shells were strongly correlated, affecting both the Fe···Fe coordination number and distance. The results were once more quite similar for **EXAFS1**, **EXAFS2**, and **EXAFS5**, but the Fe···Fe distance was shortened to 3.35–3.38 Å and the Fe···C distance was ~3.05 Å (Table III, fits 1J, 2J, and 5J). Attempts to fit the data with a 3.4 Å Fe···Fe distance and a longer Fe···C distance resulted in a second, less well-defined fit with an Fe···C distance of ~3.3 Å, and increased Fe···Fe distances of 3.45–3.47 Å (Table III, fits 1I, 2I, and 5I). Fits to the short Fe···Fe distance with the 3.05 Å Fe···C distance resulted in chemically unreasonably short Fe···Fe distances and a decrease in the Fe coordination number (Table III, fits 1K, 2K, and 5K). For **EXAFS4** the 3.4 Å Fe contribution was essentially overshadowed by the 3.04 Å Fe–C wave and showed very high correlation of the coordination numbers for the fit consisting of the long Fe/long C distances (Table III, fit 4I). The best fit occurred at a very short Fe···Fe distance with the 3.04 Å Fe···C distance (Table III, fit 4K). Fits to a shorter k range, 3.8–10.0 Å^{-1}, truncating the data to exclude the high noise level above k = 10 Å^{-1}, showed a strong preference for the long Fe···Fe distance, with F = 0.45 for the 3.4 Å distance and F = 0.79 for the 3.0 Å distance (compare with Table III, fits 4E and 4F). The C-only fit was no longer better than the long Fe···Fe fit.[53]

For the reduced samples **EXAFS3** and **EXAFS6**, the Fourier transform shows very low intensity in the second shell region of the other samples (Figure 8d,e). Fits were attempted for a variety of backtransforms. No Fe-only, C-only, or Fe + C wave could successfully fit the data.

(c) Wide Shell Fits. The same trends and distance information were obtained from fits to EXAFS spectra from wide backtransforms of the data for the oxidized and semimet protein samples [see Tables IV and S1 (Table S1 is in the supplementary material)]. All numerical values were the same, with the only significant difference occurring for the first shell N/O coordination numbers for **EXAFS1** which, due to the ambiguity in selecting a narrow Fourier filter window, had been biased toward lower values (5 vs 6). Addition of an Fe contribution to N and O was necessary to explain the metrical details of the data and improved the fit dramatically (Figure 10a,b) with the fit function dropping from a value of 1.0 for **EXAFS5** (fit 5L) to 0.52 (fit 5M). Inclusion of C further improved the fit (Figure 10c), with the fit function falling to 0.43 (Table S1, fit 5R). Although our carbon parameters are not reliable, this trend clearly shows that something

(49) Scott, R. A.; Eidsness, M. K. *Comments Inorg. Chem.* **1988**, *7*, 235–267.

(50) Cramer, S. P. Ph.D. Thesis, Stanford University, 1977.

(51) Scarrow, R. C.; Maroney, M. J.; Palmer, S. M.; Que, L., Jr.; Roe, A. L.; Salowe, S. P.; Stubbe, J. *J. Am. Chem. Soc.* **1987**, *109*, 7857–7864.

(52) In a recent study of mono- and dinuclear Cu models, difficulties in determining the presence of, and distance between, Cu and Cu/Fe in various models were found to be due in part to the ability of second shell carbon to mimic the second shell metal–metal interaction (see ref 49). In some cases, the authors found that they could fit their second shell copper dimer data with carbon only and no copper contribution, similar to what we found during second shell fits to our data.

(53) Data from 3.5–10.5 Å^{-1} were Fourier transformed and fit between 3.8 and 10 Å^{-1} for the other protein samples as well. Essentially the same distance information was obtained as for the wider range with an increase in the quality (decrease in the F values) of the fits. In general, the sum of low-Z coordination numbers dropped to closer to five and the Fe coordination numbers decreased to or just under 1 for the 3.4 Å distance. The most important differences occurred for the second shell fits. For the shorter data range, C-only fits to the data were not better than Fe-only fits, and the correlation between the Fe and C parameters was not as strong. Upon addition of C to the fits, the Fe···Fe distances stayed closer to those found for the Fe-only fits. For **EXAFS4**, the best fit to the data over the short data range consisted of 2.9 N at 2.21 Å, 3.5 O at 1.99 Å, and 0.9 Fe at 3.43 Å (Figure 11b).

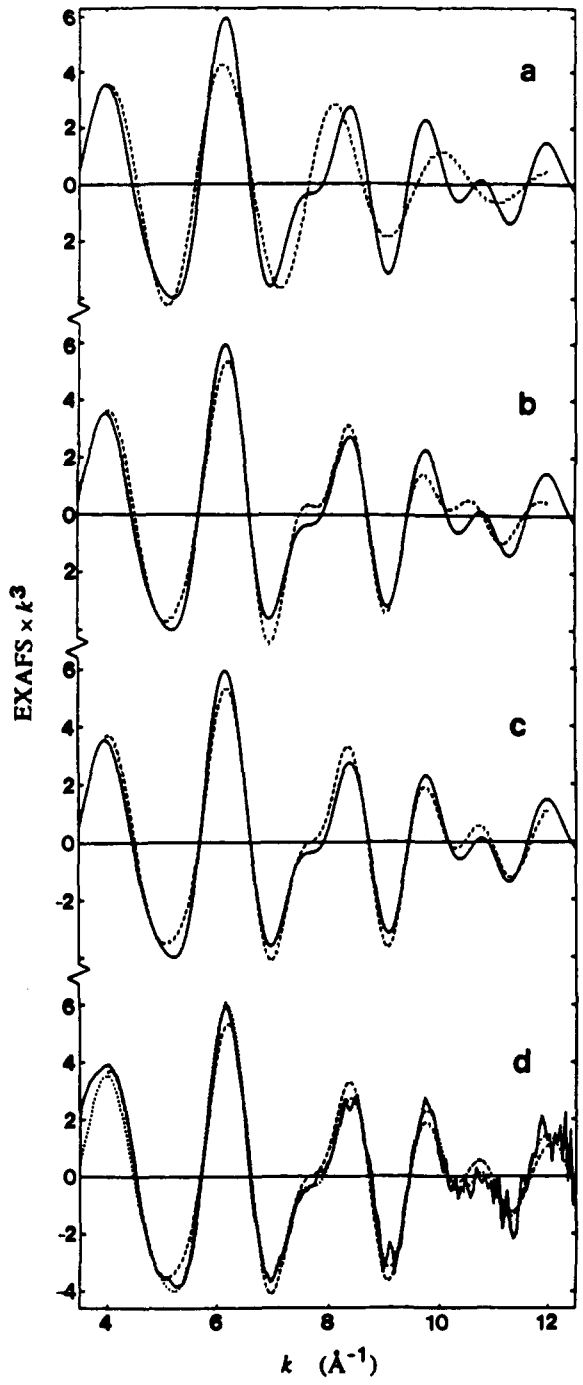

Figure 10. Fits to the Fourier filtered data for **EXAFS5**. The solid line represents the data and the dashed line is the fit. (a) Fit to the data with N and O (Table IV, fit 5L), (b) fit to the data with N, O, and Fe (Table IV, fit 5M), (c) fit to the data with N, O, Fe, and C (Table S1, fit 5R), (d) the unfiltered data (—), the filtered data (···), and the fit to the filtered data (---) (Table S1, fit 5R).

in addition to Fe is necessary to fit the data properly. Similar improvements were seen for the other samples with the above noted ambiguity in Fe vs C remaining for **EXAFS4**. A comparison of final fits with the data is given in Figure 11.[54]

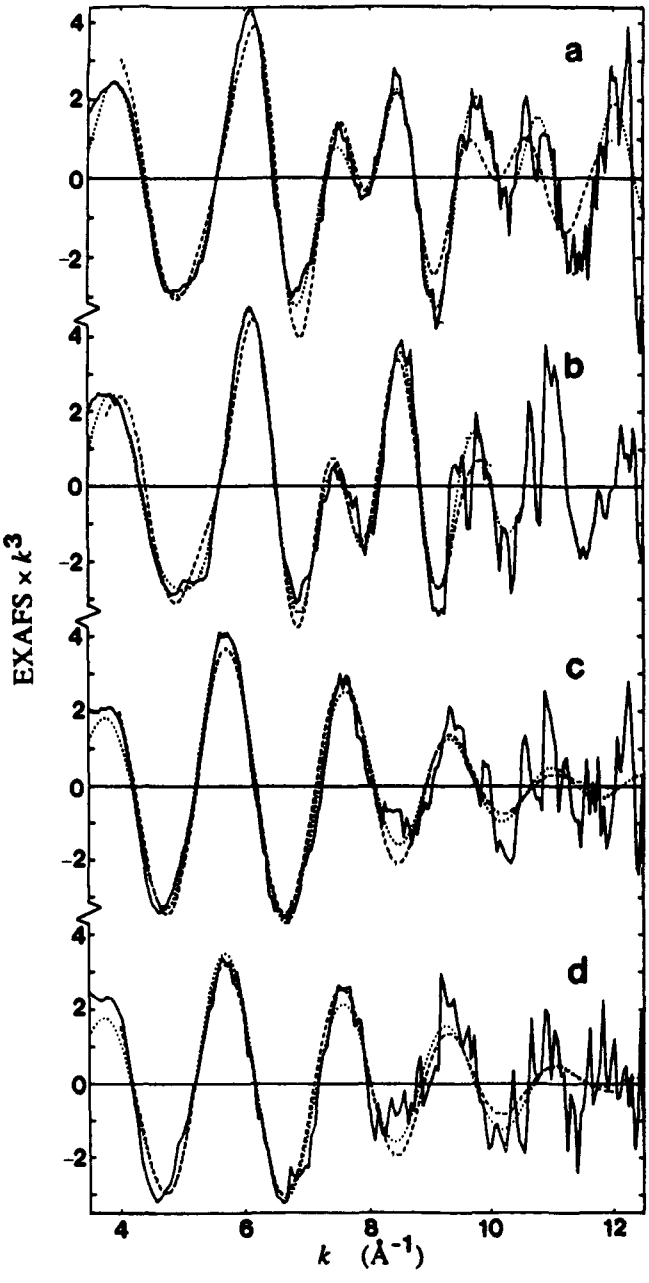

Figure 11. A comparison of the unfiltered data (—), the filtered data (···), and the fit to the filtered data (---); (a) **EXAFS2** (Table IV, fit 2M), (b) **EXAFS4** (see ref 53), (c) **EXAFS3** (Table II, fit 3C), (d) **EXAFS6** (Table II, fit 6C).

With regard to the second shell, we conclude that the most reasonable interpretation is that the shell contains an Fe backscatterer at a distance of about 3.42 Å for the oxidized and semimet samples. This distance should not be affected by intervening-atom multiple scattering effects, because the minimum Fe–O bridge distance of 2.0 Å corresponds to a maximum Fe–O–Fe angle of 129°.[55] The 3.4 Å distance is consistent with the location and large magnitude seen for the second shell peak in the Fourier transform for both the protein samples and the dinuclear Fe model complexes (see Figure 2 in ref 23). The presence of Fe in the second shell is also compatible with EPR data showing the existence of a dinuclear iron center. We believe that the spread in Fe distances found when adding a C wave to the Fe wave is an artifact of the correlation between the Fe–Fe and Fe–C parameters. For model compounds, the correct Fe···Fe distance is obtained when fitting with Fe alone, and a similar correlation effect

(54) The unfiltered data between $k = 4$ and 12 Å^{-1} were also fit. Although the quality of the fits was generally worse due to the increased noise level of the unfiltered data, the results of the fits were again similar to those for fits over the wide Fourier transform range of **EXAFS1**, **EXAFS2**, **EXAFS4**, and **EXAFS5** reported in Table IV, and to the first shell fits for **EXAFS3** and **EXAFS6** reported in Table II. Some variation in the coordination numbers for low-Z backscatterers was found, but the overall coordination information was the same as that for the filtered data fits. The fit results for the raw data, the wide shell data, and the filtered data are thus consistent.

(55) Co, M. S.; Hendrickson, W. A.; Hodgson, K. O.; Doniach, S. *J. Am. Chem. Soc.* **1983**, *105*, 1114–1150.

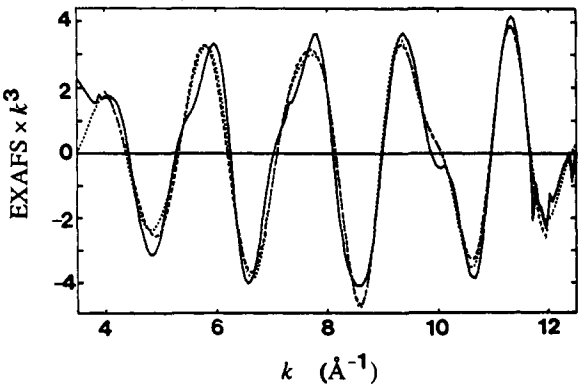

Figure 12. A comparison of the unfiltered data (—), the filtered data (···), and the best fit to the filtered data (---) for $[Fe_2O(O_2CH)_4(BIPhMe)_2]$ (Table V, fit 7L).

is seen when fitting the oxo-bridged model with the same Fe–Fe and Fe–C parameters used in the protein fits. We further conclude that there is a shell of low-Z scatterers distributed around 3.05 Å. The strength in this backscattering could arise from second shell atoms arranged in a rigid structure such as the imidazole ring (present in histidine). With Fe–N distances around 2.1–2.2 Å, the Fe–C/N second shell distances lie in the 3.0–3.2 Å range, in accord with the present observations.[56]

Plots of individual contributions to the wide shell fits showed that the differences in the EXAFS spectra at ~7 and 11 Å for the oxidized and semimet samples are caused by changes in the N/O wave interaction with a more or less constant Fe wave. For the oxidized sample, the Fe wave at ~7 and 11 Å maximizes almost directly on top of minima in the N/O wave, giving rise to the weak shoulder in the data at those two points relative to data for the semimet hydroxylase. For the semimet sample, the N/O wave has shifted to lower frequency and the Fe wave maxima at the two points in question are no longer at a location corresponding to N/O minima, resulting in peak-like features.

Model Dependence of EXAFS Results. Given that the Fe···Fe distance obtained in the fits of the oxidized and semimet protein data was similar to that of the **FeOHFe–HBpz** model used to extract Fe–Fe backscattering parameters, we investigated the possibility of model dependence of our fit results. These same parameters were therefore used to fit the data of the **FeOFe–HBpz** model compound, and parameters obtained from this model were used to fit the **FeOHFe–HBpz** data. In both cases, two Fe···Fe distances were found, the correct one and one at about 0.4 Å away, at 3.43 and 3.06 Å for **FeOHFe–HBpz** and at 3.15 and 3.52 Å for **FeOFe–HBpz**. The goodness-of-fit parameter, however, was lower for the longer distance obtained for the **FeOFe–HBpz** model with use of Fe–Fe parameters from the hydroxo-bridged model (which has a longer Fe···Fe distance) and for the shorter distance obtained for **FeOHFe–HBpz** with use of Fe–Fe parameters from the oxo-bridged model (which has a shorter Fe···Fe distance). Cross fits were performed on $[Fe_2O(O_2CH)_4(BIPhMe)_2]$ model data, and similar results were obtained. The correct distance, ~3.2 Å, and a distance of 3.55 Å were obtained, with the fit function value being lower for the short distance when the oxo-bridged Fe parameters were used and for the longer distance when the hydroxo-bridged Fe parameters were used. A strong preference for a short Fe–C wave (~3.0 Å) was obtained in both cases. *There is thus an apparent model dependence in which the correct distance is obtained but the results are biased to give preference to the wrong distance if a model much different from the unknown is employed.* Since first shell fits showed the absence of an oxo bridge, and the Fe···Fe and Fe···low-Z scattering distances are less highly correlated in **FeOHFe–HBpz** vs **FeOFe–HBpz**, we believe that the use of parameters from the hydroxo-bridged model, **FeOHFe–HBpz**, is most appropriate and that the 3.42 Å distance is correct. While the absence of an oxo bridge is clear, it remains to be established whether our current approach would successfully distinguish highly correlated Fe–Fe (~3.06 Å) and Fe–C backscattering contributions for well-characterized complexes containing the $Fe_2(OR)_2$ bridge unit.[57] The apparent model dependence of the second shell fits to the data, an effect which has also been addressed by others,[48] warrants careful consideration of the model used in the determination of Fe···Fe distances in dinuclear iron centers.

Model Compound. EXAFS of $[Fe_2O(O_2CH)_4(BIPhMe)_2]$[24] was also measured and is presented (Figure 7h) along with its Fourier transform (Figure 8f). The metrical details of the EXAFS are very similar to those of the **FeOFe–HBpz** model complex, Figure 7a, and quite different from those of the hydroxo-bridged **FeOHFe–HBpz** model complex and of the proteins. These results again illustrate the unique effect of the oxo bridge on EXAFS data. Results of fits to the data along with crystallographic information are presented in Table V. In contrast to all of the samples presented thus far, an Fe–O interaction corresponding to a bond length of 1.8 Å was essential for obtaining satisfactory first shell fits, as expected for a dinuclear iron center containing an oxo bridge. The best fit to the data gave an average environment of 5.6 N/O at 2.11 Å with 0.9 O at 1.80 Å (fit 7B) as compared to the average from the crystallographic information of 5 N/O at 2.09 Å with 1 O at 1.79 Å.

Although the anticipated Fe–Fe peak in the Fourier transform was much weaker than expected, fits to the second shell region required iron in addition to carbon. Fe–Fe parameters from the oxo-bridged model FeOFe–HBpz were used for these fits because this complex also contains an oxo bridge. The best fit to the data with iron-only occurred at an Fe···Fe distance of 3.19 Å (fit 7C), in good agreement with the crystallographically determined value of 3.20 Å. Addition of a carbon contribution to the iron improved the fit dramatically, giving 1.0 Fe at 3.18 Å and 4.0 C at 2.98 Å (fit 7F). It should be noted that a second Fe minimum was found at an Fe···Fe distance on the order of 3.5 Å (fit 7D) with a worse overall fit. Fits to a wide backtransform of the data gave similar results. Addition of an iron contribution to the N/O contribution (fit 7H) improved the fit greatly (fit 7I), but the Fe coordination number was only 0.5, while the N/O coordination was above 7. Addition of carbon to fit 7I improved the fit even more (fit 7L, Figure 12), increasing the iron contribution to 1.0 and decreasing the low-Z contribution to less than 6. A fit to the data was also possible with an Fe···Fe distance of 3.5 Å, but the quality of the fit was worse (fit 7J). Addition of C to this fit, while improving the *F* value, did not improve the low-Z or Fe contribution (fit 7N).

Discussion

Characterization of the Hydroxylase Component of MMO. (a) Protein Purification and Iron Content. The hydroxylase from *M. capsulatus* (Bath) for EXAFS samples was isolated by using stepwise ion exchange chromatography on DEAE cellulose followed by HPLC with a preparative scale gel filtration column. Satisfactory resolution of the hydroxylase from methanol dehydrogenase (MDH) was achieved by addition of 0.1 M NaCl to the buffer used in the HPLC step. Although this purification scheme afforded protein sufficiently pure for physical measure-

(56) The presence of rigid ligands has been associated with characteristic features in outer shell EXAFS and Fourier transforms derived therefrom. Because of the fixed arrangements of such outer shell ligands, multiple scattering pathways can accumulate, contributing significantly to the outer shell EXAFS. Various approaches have been put forth to deal more effectively with such contributions. Co et al. (Co, M. S.; Scott, R. A.; Hodgson, K. O. *J. Am. Chem. Soc.* **1981**, *103*, 986–988) described a semiempirical "group fit" approach to treating imidazole ligands. A more sophisticated multiple scattering-group fitting has been described by Hasnain and collaborators (see Hasnain, S. S., Ed. *Synchrotron Radiation and Biophysics*; Ellis Horwood Ltd.: Chichester, 1990; Chapters 3 and 4). The relatively weak outer shell features in the oxidized and semimet forms of MMO suggested that such groups might not be contributing strongly, given the range and quality of the current data. Thus we have not yet applied such methods. In progress are such studies on Fe models, and planned in the near future are attempts to obtain protein data of higher quality over a wider *k* range such that multiple-scattering and group fitting approaches can be applied.

(57) Snyder, B. S.; Patterson, G. S.; Abrahamson, A. J.; Holm, R. H. *J. Am. Chem. Soc.* **1989**, *11*, 5214–5223 and references therein.

Table V. Results of Fits[a] to the EXAFS Data and Structural Information for $[Fe_2O(O_2CH)_4(BIPhMe)_2]$[24a]

		N		O		Fe		C			
window width, Å	fit	CN[b]	R, Å	CN	R, Å	CN	R, Å	CN	R, Å	F[c]	
1.2–2.15	7A	0.7	2.27	3.8	2.08					0.17	
				1.0	1.78						
	7B	4.0	2.09	1.6	2.16					0.12	
				0.9	1.80						
2.15–3.3	7C					0.6	3.19			0.48	
	7D					0.5	3.53			0.60	
	7E							3.9	3.22	0.51	
	7F					1.0	3.18	4.0	2.98	0.17	
	7G					0.7	3.49	4.9	3.24	0.23	
1.2–3.3	7H	1.5	2.30	4.6	2.08					0.72	
				1.2	1.80						
	7I	1.3	2.30	4.5	2.08	0.5	3.19			0.44	
				1.1	1.80						
	7J	1.5	2.30	4.6	2.08	0.5	3.53			0.56	
				1.2	1.80						
	7K	1.3	2.31	4.5	2.08	2.08			3.9	3.21	0.43
				1.1	1.80						
	7L	0.5	2.29	3.8	2.08	1.0	3.17	4.0	2.97	0.19	
				0.9	1.78						
	7M	1.3	2.30	4.4	2.08	0.3	3.18	2.2	3.23	0.42	
				1.1	1.80						
	7N	1.1	2.30	4.3	2.08	0.6	3.49	4.5	3.24	0.20	
				1.1	1.79						

first shell coordination as determined by crystallography				second shell coordination as determined by crystallography		av coordination based on distance distribution	av coordination based on atom type
	R, Å		R, Å		R, Å		
Fe1–O	1.787	Fe2–O	1.79	Fe1···Fe2	3.201	2 N/O at 2.04 Å	2 N at 2.14 Å
Fe1–O	2.02	Fe2–O	2.03	4 C	3.008	3 N/O at 2.13 Å	3 O at 2.06 Å
Fe1–O	2.10	Fe2–O	2.10	3 C	3.157	1 O at 1.79 Å	1 O at 1.79 Å
Fe1–O	2.06	Fe2–O	2.06				
Fe1–N	2.09	Fe2–N	2.14				
Fe1–N	2.14	Fe2–N	2.19				

[a] Fitting range $k = 4–12$ Å^{-1}. Errors are estimated to be about ±0.03 Å for distances and 25% for coordination numbers.[34] [b] CN = coordination number. [c] F is defined in the Experimental Section.

ments, it poses several difficulties. The HPLC purification is time-consuming and was carried out at room temperature. Moreover, only 2 Fe atoms per protein molecule were obtained for hydroxylase purified in this manner, in contrast to the 4 Fe/protein recently reported for the *M. trichosporium* OB3b hydroxylase.[11c] These problems were addressed by separating hydroxylase from MDH by anion exchange chromatography on DEAE Sepharose CL6B. Final purification was then carried out by gel filtration on Sephacryl S-300. The entire purification could be carried out rapidly at 4 °C. Hydroxylase purified by these methods contained 2–4 Fe atoms per molecule, with 2 being the value most frequently observed. As mentioned above, specific activities of 100–300 mU/mg were typically measured and these values often decreased upon concentration.

Spectroscopic data reported in this paper were obtained for hydroxylase samples with different Fe contents. For the EXAFS samples, the Fe contents ranged from 1.7 Fe/protein for **EXAFS2** to 2.5 Fe/protein for **EXAFS5**. The Mössbauer and EPR samples contained 1.3 and 1.7 Fe/protein, respectively. Despite the diminished Fe content in the Mössbauer sample, all of the iron present appeared to be in the form of dinuclear clusters. The $g = 4.3$ signal in the EPR spectrum of oxidized hydroxylase (Figure 2), characteristic of mononuclear ferric ion, represents <5% of total Fe. The optical spectrum displayed in Figure 1 was obtained with protein containing 4 Fe/molecule and was purified by the improved procedure. Very similar EXAFS, Mössbauer, and EPR data have been obtained for samples with different Fe contents. In addition, Mössbauer and EPR spectra for the *M. capsulatus* (Bath) hydroxylase are very similar to data reported for the *M. trichosporium* OB3b hydroxylase,[11a] although the Fe contents vary. We are therefore confident that data reported here accurately reflect the properties of the dinuclear iron center of the MMO hydroxylase. It is presently unclear why the iron content and activity of the *M. capsulatus* hydroxylase are lower than those of the *M. trichosporium* protein.[11]

(b) Nature of the Bridge in the Diiron Center. Careful analysis of the EXAFS spectrum of the oxidized form of the MMO hydroxylase clearly indicates the absence of a short, 1.8 Å distance characteristic of an oxo-bridged diiron(III) center.[58] Also noteworthy for their absence were intermediate Z ligands such as thiolate sulfur or chloride ion. The Fe···Fe distance of 3.42 Å is compatible with a variety of monodentate nitrogen or oxygen bridging groups, including hydroxide, monodentate carboxylate, and alkoxide ion.[58,59] The value also implies the existence of at least one other bridging group, most likely a syn,syn bidentate carboxylate.[59] If the protein is hydroxo bridged, it is unlikely that the capping ligands would be nitrogen donors. The Mössbauer parameters also point to the presence of an unprecedented dinuclear unit in the hydroxylase protein. The quadrupole splitting parameter, $\Delta E_Q = 1.05$ mm/s, lies between those observed for iron oxo proteins and model complexes ($\Delta E_Q = 1.5–1.8$ mm/s) and for the hydroxo-bridged model complex ($\Delta E_Q = 0.25$ mm/s).[58] In tribridged diferric model complexes, a lower quadrupole splitting can be correlated with a longer Fe–O distance. The quadrupole splitting for the diferric hydroxylase may suggest an intermediate Fe–O distance. Alternatively, the iron centers might be pentacoordinate and/or highly distorted octahedral, geometric features that could also give rise to the observed quadrupole coupling constant. It should be recognized that the EXAFS results, which represent an average of two not necessarily identical Fe coordination environments, cannot readily distinguish between five- and six-coordination.

(58) Kurtz, D. M., Jr. *Chem. Rev.* **1990**, *90*, 585–606.
(59) Rardin, R. L., Jr.; Tolman, W. B.; Lippard, S. J. *New J. Chem.* **1991**, *15*, 417–430.

The EXAFS data for the photoreduced semimet, or Fe(II)-Fe(III), hydroxylase samples also indicated the absence of a bridging oxo ligand. The Fe···Fe distance was measured to be 3.41–3.43 Å. Although one would expect the Fe···Fe distance to lengthen upon reduction, our fit results do not show this trend. The EXAFS, Fourier transforms, and fit results of the Fe(II)-Fe(III) protein samples from both the *M. capsulatus* (Bath) and *M. trichosporium* OB3b samples (**EXAFS1**, **EXAFS2**, and **EXAFS4**, Figure 7d,e and Figure 8b,c) are very similar, suggesting that the diiron centers in the two hydroxylases are structurally very similar. Furthermore, the J value of -32 cm^{-1} indicates weak antiferromagnetic exchange, consistent with hydroxo, alkoxo, or monodentate carboxylato bridging ligands. Interestingly, the same coupling constant was recently measured in a Fe(II)Fe(III) mixed valent complex obtained by air oxidation of $[Fe_2(O_2CH)_4(BIPhMe)_2]$.[24b] Taken together, these results suggest that the dinuclear Fe center in the semimet form of MMO hydroxylase might contain either an alkoxo, hydroxo, or monodentate carboxylato bridge. Moreover, a comparison of Fe–O_{oxo} distances in the five-coordinate complexes $[Fe^{III}(acacen)]_2O$ (Fe–O_{oxo} = 1.78 Å) and $Na\{[Fe^{II,III}(acacen)]_2O\}_2$ (Fe–O_{oxo} = 2.00, 2.07 Å)[60] indicates that metalation, as well as protonation, of an oxo bridge can lengthen the Fe–oxo distance in the mixed valent state. Interestingly, this latter complex exhibits a magnetic moment of 3.64 μ_B at 290 K, which corresponds to $J \approx -30$ cm^{-1},[51] close to the value measured for the *M. capsulatus* hydroxylase.

No Fe···Fe distance could be determined from an analysis of the EXAFS spectrum of the diferrous form of the hydroxylase. The absence of a resolvable Fe···Fe interaction in diiron(II) and other reduced dinuclear metalloprotein cores and their model complexes is not unusual. In deoxyhemerythrin, the Fe···Fe second shell peak disappears upon warming the protein from 80 K to room temperature.[61] Also, no Cu(I)–Cu(I) peak is seen in the Fourier transform of deoxyhemocyanin data.[62] In addition, the Fe···Fe peak cannot be resolved in the semimet form (pink) of purple acid phosphatase.[63] This phenomenon might be caused by the loss of a bridging ligand upon reduction, resulting in uncorrelated vibrations of the metal atoms (increased Debye–Waller factor), or by destructive interference in the second shell EXAFS between the Fe···Fe wave and second shell Fe···N, Fe···C, and/or Fe···O waves.

(c) Nature of the Nonbridging Ligands. Apart from determining the nature of the bridge and the Fe···Fe separation in the MMO hydroxylase, EXAFS spectroscopy offers some information about the coordination number and ligand atom types of the iron atoms. As suggested above, one possible interpretation of the Mössbauer data is that the hydroxylase is symmetrically substituted with a coordination number of five around each atom. Although fits to the first shell EXAFS of the diferric protein suggest that the coordination number of the iron is six, the inherent uncertainty in EXAFS coordination number determination allows for one or both Fe sites to be five-coordinate. In addition, in fits to the smaller data range for the protein samples, the nitrogen coordination numbers were lower than the values obtained in the k = 4–12 Å^{-1} fits. We cannot, therefore, rule out the possibility of one or two pentacoordinate iron atoms in the dinuclear active site of MMO based on the EXAFS results. We are currently investigating the 1s → 3d pre-edge features of the diferric, diferrous, and semimet protein samples as well as a variety of dinuclear iron model compounds to gain more information about the coordination of iron in the MMO hydroxylase protein.

Comparison to Proteins and Model Complexes Containing Diiron Cores. Structural, magnetic, and spectroscopic properties of selected dinuclear iron oxo proteins and model compounds are shown in Table VI. The quadrupole splitting in the Mössbauer spectrum of the hydroxylase diferric center is closest to that reported for uteroferrin-PO_4 ($\Delta E_Q(1)$ = 1.02 mm/s, $\Delta E_Q(2)$ = 1.38 mm/s),[64] in which the presence of an oxo bridge is not clearly established. For the diferrous form, the MMO hydroxylase exhibits a quadrupole splitting similar to that of RRB2 and to the model compounds $[Fe_2(BPMP)(OPr)_2](BPh_4)$ (ΔE_Q = 2.72 mm/s)[65] and $[Fe_2(O_2CH)_4(BIPhMe)_2]$ ($\Delta E_Q(1)$ = 2.56 mm/s, $\Delta E_Q(2)$ = 3.30 mm/s).[24] The larger quadrupole splitting in the latter has been attributed to the less symmetrical pentacoordinate iron center. The Mössbauer spectrum of the diferrous hydroxylase can be fit with a single quadrupole doublet having a large splitting (ΔE_Q = 3.01 mm/s at 80 K, ΔE_Q = 3.14 mm/s at 4.2 K[11a]) which may suggest that the diiron center is symmetrically coordinated by five ligands at each iron site. Both the diiron(II) models and the reduced hydroxylase exhibit low field EPR signals. Interestingly, the third known diferrous model compound, $[Fe_2(OH)(OAc)_2(Me_3TACN)_2](ClO_4)$,[66] which contains a hydroxo rather than formato or phenoxo bridge, lacks this EPR signal.

EXAFS studies of Hr[48,67] and RRB2[51,68] have suggested that the two proteins possess similar active sites, consisting of a pair of triply bridged iron atoms at a separation on the order of 3.2 Å in the diferric form, with one oxo bridge and two carboxylate bridges. Recently, crystallographic characterization of RRB2 revealed the presence of one, not two, bridging carboxylates.[69] The average first shell coordination of oxyHr consists of 5 non-bridging N/O at 2.15–2.16 Å while the average first shell coordination of diferric RRB2 consists of 5 non-bridging N/O at 2.04–2.06 Å. In general, Fe–N bonds are longer than Fe–O bonds in iron complexes; the shorter average distance in the first shell coordination of RRB2 compared to oxyHr suggests that there are fewer nitrogens and more oxygens coordinated to iron in RRB2 than in oxyHr.[68] The crystal structure[69] has confirmed that there are just two histidine ligands coordinated to the iron atoms in RRB2, as compared to 5 histidines ligated to the diiron center in Hr. The average distance in the first coordination shell of the diferric form of MMO is 2.04 Å, suggesting that, like RRB2, there are more oxygens and fewer nitrogens coordinated to iron in MMO than in oxyHr. Unlike both diferric centers in RRB2 and oxyHr, there

(60) Arena, F.; Floriani, C.; Chiesi-Villa, A.; Guastini, C. *J. Chem. Soc., Chem. Commun.* **1986**, 1369–1371.
(61) Elam, W. T.; Stern, E. A.; McCallum, J. D.; Sanders-Loehr, J. *J. Am. Chem. Soc.* **1983**, *105*, 1919–1923.
(62) Co, M. S.; Hodgson, K. O. *J. Am. Chem. Soc.* **1981**, *103*, 3200–3201.
(63) Kauzlarich, S. M.; Teo, B. K.; Zirino, T.; Burman, S.; Davis, J. C.; Averill, B. A. *Inorg. Chem.* **1986**, *25*, 2781–2785.
(64) Pyrz, J. W.; Sage, J.; Debrunner, P. G.; Que, L., Jr. *J. Biol. Chem.* **1986**, *261*, 11015–11020.
(65) Borovik, A. S.; Que, L., Jr. *J. Am. Chem. Soc.* **1988**, *110*, 2345–2347.
(66) Hartman, J. R.; Rardin, R. L.; Chaudhuri, P.; Pohl, K.; Wieghardt, K.; Nuber, B.; Weiss, J.; Papaefthymiou, G. C.; Frankel, R. B.; Lippard, S. J. *J. Am. Chem. Soc.* **1987**, *109*, 7387–7396.
(67) Elam, W. T.; Stern, E. A.; McCallum, J. D.; Sanders-Loehr, J. *J. Am. Chem. Soc.* **1982**, *104*, 6369–6373.
(68) (a) Scarrow, R. C.; Maroney, M. J.; Palmer, S. M.; Que, L., Jr.; Salowe, S. P.; Stubbe, J. *J. Am. Chem. Soc.* **1986**, *108*, 6832–6834. (b) Bunker, G.; Petersson, L.; Sjöberg, B.-M.; Sahlin, M.; Chance, M.; Chance, B.; Ehrenberg, A. *Biochemistry* **1987**, *26*, 4708–4716.
(69) Nordlund, P.; Sjöberg, B.-M.; Eklund, H. *Nature* **1990**, *345*, 593–598.
(70) Hendrickson, W. A.; Co, M. S.; Smith, J. L.; Hodgson, K. O.; Klippenstein, G. L. *Proc. Natl. Acad. Sci. USA* **1982**, *79*, 6255–6259.
(71) Stenkamp, R. E.; Sieker, L. C.; Jensen, L. H. *J. Am. Chem. Soc.* **1984**, *106*, 618–622.
(72) (a) Dawson, J. W.; Gray, H. B.; Hoenig, H. E.; Rossman, G. R.; Schredder, J. M.; Wang, R. H. *Biochemistry* **1972**, *11*, 461–465. (b) Garbett, K.; Darnell, D. W.; Klotz, I. M.; Williams, R. J. P. *Arch. Biochem. Biophys.* **1969**, *103*, 419–434.
(73) Clark, P. E.; Webb, J. *Biochemistry* **1981**, *20*, 4628–4632.
(74) Atkin, C. L.; Thelander, L.; Reichard, P.; Lang, G. *J. Biol. Chem.* **1973**, *248*, 7464–7472.
(75) Debrunner, P. G.; Hendrich, M. P.; deJersey, J.; Keough, D. T.; Sage, J. T.; Lerner, B. *Biochim. Biophys. Acta* **1983**, *745*, 103–106.
(76) Lauffer, R. B.; Antanaitis, B. C.; Aisen, P.; Que, L., Jr. *J. Biol. Chem.* **1983**, *258*, 14212–14218.
(77) (a) Marini, P. J.; Murray, K. S.; West, B. O. *J. Chem. Soc., Chem. Commun.* **1981**, 726–728. (b) Marini, P. J.; Murray, K. S.; West, B. O. *J. Chem. Soc., Dalton Trans.* **1983**, 143–151.
(78) Day, E. P.; David, S. S.; Peterson, J.; Dunham, W. R.; Bonvoisin, J. J.; Sands, R. H.; Que, L., Jr. *J. Biol. Chem.* **1988**, *263*, 15561–15567.
(79) Maroney, M. J.; Kurtz, D. M., Jr.; Nocek, J. M.; Pearce, L. L.; Que, L., Jr. *J. Am. Chem. Soc.* **1986**, *108*, 6871–6879.
(80) Lynch, J. B.; Juarez-Garcia, C.; Münck, E.; Que, L., Jr. *J. Biol. Chem.* **1989**, *264*, 8091–8096.
(81) Sahlin, M.; Gräslund, A.; Petersson, L.; Ehrenberg, A. Sjöberg, B.-M. *Biochemistry* **1989**, *28*, 2618–2625.
(82) Que, L., Jr.; True, A. E. *Prog. Inorg. Chem.* **1990**, *38*, 97–200.

Table VI. Structural, Mössbauer, and Magnetic Properties of Selected Diiron Proteins and Model Complexes

Fe(III)Fe(III)

protein	ref	Fe–μ–O, Å	Fe···Fe, Å	Fe–O–Fe, deg	Fe–O,N, Å	J, cm^{-1}	δ, mm/s	ΔE_q, mm/s
M. capsulatus (Bath) hydroxylase	this work		3.42		2.04	−32	0.50	1.05
M. trichosporium OB3b hydroxylase	11a						0.50	1.07
methemerythrin	48, 51, 67, 68a, 70, 71, 72	1.76–1.80	3.20–3.24	~127	2.10–2.15	−134	0.46	1.57
oxyhemerythrin	48, 67, 72a, 73	1.82	3.24	~128	2.17	−77	0.51	1.96
							0.52	0.95
native RRB2	51, 68, 69, 74	1.78–1.80	3.21–3.26	~130	2.04–2.06	−108	0.53	1.65
							0.45	2.45
purple acid phosphatase (purple)	63		3.00		2.05			
uteroferrin	64, 76					≤−40	0.55	1.65
							0.46	2.12
uteroferrin-PO_4	64, 82		3.1–3.2		1.96		0.52	1.02
					2.10		0.55	1.38

model compound	ref	Fe–μ–O, Å	Fe···Fe, Å	Fe–O–Fe, deg	Fe–O_{car}, Å	Fe–N_{cis}, Å	Fe–N_{trans}, Å	J, cm^{-1}	δ, mm/s	ΔE_Q, mm/s
$[Fe_2O(OAc)_2(HB(pz)_3)_2]$	38a	1.78	3.146	123.6	2.04	2.15	2.19	−121	0.52	1.60
$[Fe_2OH(OAc)_2(HB(pz)_3)_2](ClO_4)$	38b	1.96	3.439	124	2.00	2.10	2.10	−17	0.47	0.25
$[Fe(tsalen)]_2Opy$	77b	1.78	3.53	159		2.06	2.06	−100 (calc)		
$[Fe_2O(O_2CH)_4(BIPhMe)_2]$	24b	1.80	3.21	126.6		2.12	2.17	−111	0.54	1.81
		1.79								

Fe(II)Fe(III)

protein	ref	Fe–μ–O, Å	Fe···Fe, Å	Fe–O–Fe, deg	Fe–O,N, Å	J, cm^{-1}	δ, mm/s	ΔE_Q, mm/s
M. capsulatus (Bath) hydroxylase	this work		3.41–3.43		2.06–2.09	−32		
M. trichosporium OB3b hydroxylase	this work, 41		3.42		2.06	−30		
semimethemerythrin N_3	45, 51, 68a	1.87	3.46	135	2.14	−15		
purple acid phosphatase (pink)	63				2.08			
$uteroferrin_{red}$	75, 78, 82				2.02	−9.9	0.53	1.78
					2.13		1.22	2.63

model compound	ref	Fe–μ–O, Å	Fe···Fe, Å	Fe–O–Fe, deg	Fe–N_{cis}, Å	Fe–N_{trans} Å	J, cm^{-1}	δ, mm/s	ΔE_Q, mm/s
$[Fe_2(BPMP)(OPr)_2](BPh_4)_2$	65	1.94	3.36	113.1	2.17	2.13		0.48	0.50
		2.09			2.18	2.14		1.13	2.69
$\{Na[Fe^{II,III}(acen)_2]_2O\}_2$	60	2.09	3.76	134.9			−30 (calc)		
		2.07							

Fe(II)Fe(II)

protein	ref	Fe–μ–O, Å	Fe···Fe, Å	Fe–O–Fe, deg	Fe–O,N, Å	J, cm^{-1}	δ, mm/s	ΔE_Q, mm/s
M. capsulatus (Bath) hydroxylase	this work				2.15–2.16		1.30	3.014 (80 K)
M. trichosporium OB3b hydroxylase	11a						1.30	3.14 (4.2 K)
deoxyhemerythrin	48, 61, 67, 73, 79	1.98	3.57	128	2.19	~15	1.14	2.76
RRB2 (reduced)	80, 81					~5	1.26	3.13

model compound	ref	Fe–μ–O, Å	Fe···Fe, Å	Fe–O–Fe, deg	Fe–N_{cis}, Å	Fe–N_{trans}, Å	J, cm^{-1}	δ, mm/s	ΔE_Q, mm/s
$[Fe_2(OCH)_4(BIPhMe)_2]$	24a,b	2.11	3.57	113.0			~0	1.26	2.56
		2.17						1.25	3.30
$[Fe_2(OH)(OAc)_2(Me_3TACN)]ClO_4$	66	1.99	3.32	113.2	2.28	2.30	−13	1.16	2.83
$[Fe_2(BPMP)(OPr)_2](BPh_4)$	65	2.06	3.35	108.9	2.25	2.17	>0	1.20	2.72

is no oxo bridge in the dinuclear iron center of MMO, and the Fe···Fe distance, determined to be 3.42 Å, is longer than the Fe···Fe distance in either of these proteins, as one would expect for a di- or tri-bridged complex without an oxo bridge. The different optical spectra of the Fe(III)Fe(III) cores in MMO hydroxylase and RRB2 further indicate that the detailed structures of their cores must differ.

No evidence for an oxo bridge was found in the diferric form of PAP (purple acid phosphatase), although the presence of short Fe–O (tyrosine) bonds in the protein could have obscured the contribution in the Fe–O (bridge) chromophore to the data.[63] Thus, the possibility of an oxo bridge could not be ruled out. An Fe···Fe distance of 3.00 Å was deduced by the FABM curve fitting technique with parameters obtained by using a mono-bridged (μ-oxo)diiron(III) model compound.[63] The first shell coordination was similar to that reported here for MMO (Table II, fit 5C), with 3.0 N/O at 2.13 Å and 3.5 N/O at 1.98 Å, or an average of 6.5 N/O at 2.05 Å. Similarly, the EXAFS experiment on oxidized MMO from *Methylobacterium* CRL-26 indicated an Fe···Fe distance of 3.05 Å by using model corrected theoretical amplitude and phase parameters, while no evidence for or against an oxo bridge in the first shell was found owing to the limited range of the data.[9] This value disagrees with the Fe···Fe distance found in the present study for the same protein from a different species. Although it is possible that this difference is real, implying structurally different dinuclear iron centers, we suggest that the discrepancy may arise from differences in analysis protocol. The first shell coordination of the hydroxylase from *Methylobacterium* CRL-26 consisted of 4–6 N/O at an average distance of 1.92 Å. This distance is much shorter than that found for any other diferric protein.

The average increase of 0.04 Å in the first shell coordination distance upon photoreduction to the semimet state of MMO is similar to the increase in the average coordination sphere for oxidized PAP (purple) upon conversion to its one electron reduced (pink) form (6.0 N/O at 2.08 Å).[63] The Fe···Fe distance of 3.41–3.43 Å is slightly shorter than the Fe···Fe distance found for semimethemerythrin azide.[51]

The average first shell coordination distance increased by an average of 0.12 Å from the diferric to the diferrous state. The data and fits for the two diferrous protein samples are essentially identical, although **EXAFS3** had higher coordination numbers than **EXAFS6**. For deoxyhemerythrin, the average first shell coordination was 2.15 Å by EXAFS analysis, and the average first shell coordination of the diferrous hydroxylase, 2.15 Å, is in good agreement with that number. The peak associated with the metal-metal interaction is missing for both reduced hydroxylase protein samples, suggesting that the absence of a Fe···Fe backscattering peak is inherent in the structure of the samples, and not an artifact of the data collection or analysis. A 3.57 Å Fe···Fe distance has been reported for deoxyhemerythrin.[48]

Conclusions. While initial EPR studies suggested that the active site of the MMO hydroxylase is similar to the dinuclear iron centers found in Hr and RRB2, our results indicate some striking differences. The hydroxylase does not contain an oxo-bridged diiron core like that observed in Hr and RRB2. The 3.4 Å Fe···Fe distance, the intermediate Mössbauer quadrupole splitting, the semimet J value of -32 cm^{-1}, and the featureless absorption spectrum indicate that the hydroxylase contains a novel Fe···Fe bridge. We believe that the diiron center may contain an alkoxo, a hydroxo, or a monodentate carboxylato bridge, and one or two bidentate bridging carboxylates. The coordination of the Fe atoms has yet to be conclusively determined. We have also reported a model dependence for EXAFS results, which has important implications for the determination of Fe···Fe distances by EXAFS.

Acknowledgment. The data were collected at the Stanford Synchrotron Radiation Laboratory and the National Synchrotron Light Source, Brookhaven National Laboratory, which are supported by the Department of Energy, Office of Basic Energy Sciences, Division of Chemical Sciences and Division of Materials Sciences. SSRL is also supported by the National Institutes of Health, Biomedical Resource Technology Program, Division of Research Resources (RR-01209). Grant support was provided by the National Science Foundation (CHE 88-17702 to K.O.H.), the Gas Research Institute (5086-260-1209 to H.D.), and the National Institute of General Medical Sciences (GM 32134 to S.J.L.). J.G.B. acknowledges support as an American Cancer Society Postdoctoral Fellow. $[Fe_2O(O_2CH)_4(BIPhMe)_2]$ was kindly provided by Dr. William B. Tolman.

Registry No. Fe, 7439-89-6; $[Fe_2O(O_2CH)_4(BIPhMe)_2]$, 123594-49-0; hydroxylase, 9046-59-7; methane monooxygenase, 51961-97-8.

Supplementary Material Available: Table S1 giving results of wide shell fits to the hydroxylase (2 pages). Ordering information is given on any current masthead page.

Control of Magnetic Interactions in Polyarylmethyl Triplet Diradicals Using Steric Hindrance

Andrzej Rajca,*,† Suchada Utamapanya, and Jiangtien Xu

Contribution from the Department of Chemistry, Kansas State University, Manhattan, Kansas 66506. *Received May 17, 1991. Revised Manuscript Received July 26, 1991*

Abstract: Three polyarylmethyl triplet diradicals are prepared by oxidation of the corresponding carbodianions. Solid-state studies of the diradicals using SQUID show an onset of short-range ferromagnetic interactions at temperatures below 4 K for diradical $3^{2\bullet}$ and antiferromagnetic interactions below 70 K for diradicals $2^{2\bullet}$ and $4^{2\bullet}$. The diradicals and the corresponding carbodianions in solution are characterized using ESR, NMR, and UV-vis spectroscopy, and voltammetry.

Introduction

Organic magnets may offer a novel insight into the nature of magnetism and may lead to materials with combined unusual optical, electrical, and magnetic properties.[1] In most organic molecular solids composed of open-shell molecules, the unpaired electrons interact weakly and, if a significant interaction takes place, it is usually antiferromagnetic. Such solids are either bulk paramagnets or, if antiferromagnetic interactions lead to a long-range ordering of unpaired spins, antiferromagnets. Several exceptional organic solids have been found to possess weak ferromagnetic intermolecular interactions: dinitroxy,[2] nitronyl oxide,[3] galvinoxyl,[4] and nitrophenyl verdazyl.[5] However, none of these solids is a ferromagnet. Ferromagnetic interactions are prerequisite to most interesting magnetic properties.[6] Thus, the ability to design solids with ferromagnetic interactions in a rational manner is important and intellectually challenging.

In 1963, McConnell used a simple theory to propose that a nearest-neighbor π-overlap of the sites with the opposite sign spin densities located at adjacent molecules should lead to intermolecular ferromagnetic coupling.[7] Many π-conjugated radicals and polyradicals possess such alternating sign spin densities.[8] Izuoka, Murata, Sugawara, and Iwamura showed that the coupling between two triplet carbenes in a cyclophane framework can be predicted using the McConnell model.[9] Similarly, the ferromagnetic vs antiferromagnetic coupling was correlated with X-ray structures for two solid monoradicals.[5]

Now we report the preparation, spectroscopy, and solid-state studies on triplet diradicals $2^{2\bullet}$, $3^{2\bullet}$, and $4^{2\bullet}$ (Figure 1). $2^{2\bullet}$, $3^{2\bullet}$, and $4^{2\bullet}$ are derivatives of previously reported diradicals $1^{2\bullet}$, Schlenk hydrocarbon $5^{2\bullet}$, and perchlorinated Schlenk hydrocarbon.[10-12]

† The Camille and Henry Dreyfus Teacher-Scholar, 1991.

(1) Carter, F. L., Ed. *Molecular Electronic Devices*; Marcel Dekker: New York, 1982 and 1987; Vols. I and II.
(2) Saint Paul, M.; Veyret, C. *Phys. Lett. A* **1973**, *45*, 362. Chouteau, G.; Veyret-Jeandey, C. *J. Phys.* **1981**, *42*, 1441.
(3) Awaga, K.; Maruyama, Y. *Chem. Phys. Lett.* **1989**, *158*, 556. Awaga, K.; Maruyama, Y. *J. Chem. Phys.* **1989**, *91*, 2743. Awaga, K.; Inabe, T.; Nagashima, U.; Maruyama, Y. *J. Chem. Soc., Chem. Commun.* **1989**, 1617; **1990**, 520.
(4) Awaga, K.; Sugano, T.; Kinoshita, M. *J. Chem. Phys.* **1986**, *85*, 2211. Kinoshita, M. *Mol. Cryst. Liq. Cryst.* **1990**, *176*, 163.
(5) Allemand, P.-M.; Srdanov, G.; Wudl, F. *J. Am. Chem. Soc.* **1990**, *112*, 9391. The correlation is between room temperature structure and magnetic interactions in the liquid helium temperature range.
(6) Carlin, R. L. *Magnetochemistry*; Springer-Verlag: Berlin, 1986.
(7) McConnell, H. M. *J. Chem. Phys.* **1963**, *39*, 1910.
(8) Mataga, N. *Theor. Chim. Acta* **1968**, *10*, 372. Ovchinnikov, A. A. *Theor. Chim. Acta* **1978**, *47*, 497. Wertz, J. E.; Bolton, J. R. *Electron Spin Resonance*; Chapman: New York, 1986; Chapter 6.
(9) Izuoka, A.; Murata, S.; Sugawara, T.; Iwamura, H. *J. Am. Chem. Soc.* **1987**, *109*, 2631.
(10) Rajca, A. *J. Am. Chem. Soc.* **1990**, *112*, 5890.

0002-7863/91/1513-9235$02.50/0